Commun. Comput. Phys.
doi: 10.4208/cicp.250112.061212a

Vol. **14**, No. 3, pp. 819-850
September 2013

Numerical Study of Quantized Vortex Interaction in the Ginzburg-Landau Equation on Bounded Domains

Weizhu Bao[1,*] and Qinglin Tang[1]

[1] *Department of Mathematics and Center for Computational Science and Engineering, National University of Singapore, Singapore 119076.*

Received 25 January 2012; Accepted (in revised version) 6 December 2012

Communicated by Qiang Du

Available online 6 March 2013

Abstract. In this paper, we study numerically quantized vortex dynamics and their interaction in the two-dimensional (2D) Ginzburg-Landau equation (GLE) with a dimensionless parameter $\varepsilon > 0$ on bounded domains under either Dirichlet or homogeneous Neumann boundary condition. We begin with a review of the reduced dynamical laws for time evolution of quantized vortex centers in GLE and show how to solve these nonlinear ordinary differential equations numerically. Then we present efficient and accurate numerical methods for discretizing the GLE on either a rectangular or a disk domain under either Dirichlet or homogeneous Neumann boundary condition. Based on these efficient and accurate numerical methods for GLE and the reduced dynamical laws, we simulate quantized vortex interaction of GLE with different ε and under different initial setups including single vortex, vortex pair, vortex dipole and vortex lattice, compare them with those obtained from the corresponding reduced dynamical laws, and identify the cases where the reduced dynamical laws agree qualitatively and/or quantitatively as well as fail to agree with those from GLE on vortex interaction. Finally, we also obtain numerically different patterns of the steady states for quantized vortex lattices under the GLE dynamics on bounded domains.

AMS subject classifications: 35Q56, 65M06, 65M70, 82D55

Key words: Ginzburg-Landau equation, quantized vortex, Dirichlet boundary condition, homogeneous Neumann boundary condition, reduced dynamical laws, time splitting, compact finite difference method, finite element method.

1 Introduction

A quantized vortex in two-dimensional (2D) space is a particle-like or topological defect, whose center is zero of the order parameter, possessing localized phase singularity with

*Corresponding author. *Email addresses:* bao@math.nus.edu.sg (W. Bao), tqltql2010@gmail.com (Q. Tang)

integer topological charge called also as winding number or index. Quantized vortices have been widely observed in many different physical systems, such as the liquid helium, type-II superconductors, Bose-Einstein condensates, atomic gases and nonlinear optics [1, 5, 10, 12, 23, 28]. They are key signatures of superconductivity and superfluidity and their study retains as one of the most important and fundamental problems since they were predicted by Lars Onsager in 1947 in connection with superfluid Helium.

In this paper, we are concerned with the vortex dynamics and interactions in 2D Ginzburg-Landau equation (GLE) for modelling superconductivity [15, 23, 25]:

$$\lambda_\varepsilon \partial_t \psi^\varepsilon(\mathbf{x},t) = \Delta\psi^\varepsilon + \frac{1}{\varepsilon^2}(1-|\psi^\varepsilon|^2)\psi^\varepsilon, \qquad \mathbf{x}\in\Omega, \quad t>0, \tag{1.1}$$

with initial condition

$$\psi^\varepsilon(\mathbf{x},0) = \psi_0^\varepsilon(\mathbf{x}), \qquad \mathbf{x}\in\bar{\Omega}, \tag{1.2}$$

and under either Dirichlet boundary condition (BC)

$$\psi^\varepsilon(\mathbf{x},t) = g(\mathbf{x}) = e^{i\omega(\mathbf{x})}, \qquad \mathbf{x}\in\partial\Omega, \quad t\geq 0, \tag{1.3}$$

or homogeneous Neumann BC

$$\frac{\partial\psi^\varepsilon(\mathbf{x},t)}{\partial\mathbf{n}} = 0, \qquad \mathbf{x}\in\partial\Omega, \quad t\geq 0. \tag{1.4}$$

Here, $\Omega\subset\mathbb{R}^2$ is a 2D smooth and bounded domain, t is time, $\mathbf{x}=(x,y)\in\mathbb{R}^2$ is the Cartesian coordinate vector, $\psi^\varepsilon := \psi^\varepsilon(\mathbf{x},t)$ is a complex-valued function describing the 'order parameter' for a superconductor, ω is a given real-valued function, ψ_0^ε and g are given smooth and complex-valued functions satisfying the compatibility condition $\psi_0^\varepsilon(\mathbf{x})=g(\mathbf{x})$ for $\mathbf{x}\in\partial\Omega$, $\mathbf{n}=(n_1,n_2)$ and $\mathbf{n}_\perp=(-n_2,n_1)\in\mathbb{R}^2$ satisfying $|\mathbf{n}|=\sqrt{n_1^2+n_2^2}=1$ are the outward normal and tangent vectors along $\partial\Omega$, respectively, $\varepsilon>0$ is a given dimensionless constant, and λ_ε is a positive function of ε. Denote the Ginzburg-Landau (GL) functional ('energy') as [15, 23, 25]

$$\mathcal{E}^\varepsilon(t) := \int_\Omega \left[\frac{1}{2}|\nabla\psi^\varepsilon|^2 + \frac{1}{4\varepsilon^2}\left(|\psi^\varepsilon|^2-1\right)^2\right] d\mathbf{x} = \mathcal{E}^\varepsilon_{\rm kin}(t) + \mathcal{E}^\varepsilon_{\rm int}(t), \qquad t\geq 0, \tag{1.5}$$

where the kinetic and interaction parts are defined as

$$\mathcal{E}^\varepsilon_{\rm kin}(t) := \frac{1}{2}\int_\Omega |\nabla\psi^\varepsilon|^2 d\mathbf{x}, \quad \mathcal{E}^\varepsilon_{\rm int}(t) := \frac{1}{4\varepsilon^2}\int_\Omega \left(|\psi^\varepsilon|^2-1\right)^2 d\mathbf{x}, \qquad t\geq 0,$$

then it is easy to see that, for GLE (1.1) with either Dirichlet BC (1.3) or homogeneous Neumann BC (1.4) for general domain Ω, or periodic BC when Ω is a rectangle, the GL functional decreases when time increases, i.e.

$$\frac{d}{dt}\mathcal{E}^\varepsilon(t) = -\lambda_\varepsilon\int_\Omega |\partial_t\psi^\varepsilon|^2 d\mathbf{x} \leq 0, \qquad t\geq 0.$$

There have been many analytical and numerical studies recently that deal with quantized vortex states and their interaction of the GLE (1.1) in the whole space $\mathbb{R}^2$ or on bounded domains under different scalings regarding to the distances between different vortices. Neu [28] studied vortex states and their stability of the GLE (1.1) in the whole space $\mathbb{R}^2$ with $\lambda_\varepsilon = \varepsilon = 1$ for superconductivity. Under this scaling, the vortex core size is $\mathcal{O}(1)$. He found numerically that quantized vortices with winding number $m = \pm 1$ are dynamically stable, and respectively, $|m| > 1$ dynamically unstable [28]; and obtained formally the reduced dynamical laws governing the motion of the vortex centers under the assumption that these vortices are distinct and well-separated, i.e. the reduced dynamical laws are asymptotically valid when the distances between vortices become larger and larger [28]. Based on the reduced dynamical laws which are sets of ordinary differential equations (ODEs) for the vortex centers, one can obtain that two vortices with opposite winding number attract each other, while the ones with the same winding number repel. Recently, by proposing efficient and accurate numerical methods for discretizing the GLE in the whole space, Zhang et al. [37, 38] compared the dynamics of quantized vortices from the reduced dynamical laws obtained by Neu with those from the direct numerical simulation results from GLE under different parameter and/or initial setups. They identified numerically the parameter regimes for quantized vortex dynamics when the reduced dynamical laws agree qualitatively and/or quantitatively and fail to agree with those from GLE dynamics [37, 38].

Neu's results were extended to the GLE with impurities by Jian et al. [16–18] or on bounded domain with different BCs by Lin [23–25] and the full Ginzburg-Landau model by Peres & Rubinstein [29] and later by E [12] by introducing a small dimensionless parameter $0 < \varepsilon < 1$ which is proportional to the core size of a vortex. In these extensions, the authors obtained the reduced dynamical laws for the dynamics of vortices under the GLE dynamics when $\varepsilon \to 0$ with fixed distances between different vortices initially, see for instance [2, 3, 8, 11, 25–27] and references therein. In fact, for the GL functional (1.5), Bethuel et al. [7] obtained rigorously that the core size of each vortex is of $\mathcal{O}(\varepsilon)$ when $0 < \varepsilon \ll 1$. In addition, formal analysis indicate that, if initially ψ_0^ε has isolated vortices, these vortices move with velocities of the order of $|\ln\varepsilon|^{-1}$ in the GLE (1.1) dynamics with $\lambda_\varepsilon = 1$ [6, 23, 24]. Therefore, to obtain nontrivial vortex dynamics, in this paper and from now on, we always assume $0 < \varepsilon < 1$ and choose

$$\lambda_\varepsilon = \frac{1}{|\ln\varepsilon|} = \frac{1}{\ln(1/\varepsilon)}, \qquad 0 < \varepsilon < 1. \tag{1.6}$$

In fact, for the GLE (1.1) with λ_ε chosen in (1.6) on a bounded domain, if initially ψ_0^ε has isolated vortices, when $\varepsilon \to 0$, the reduced dynamical laws for vortex centers have been obtained formally and rigorously for different boundary conditions by many authors, see for instance [6, 9, 12, 14, 15, 21, 25, 30, 36] and references therein.

The main aims of this paper are: (i) to present efficient and accurate numerical methods for discretizing the reduced dynamical laws governing the motion of vortex centers and the GLE (1.1) on either a rectangle or a disk under different BCs, (ii) to study numer-

ically vortex interaction under the GLE dynamics with different initial setups and compare them with those from the reduced dynamical laws in different parameter regimes, and (iii) to identify the cases where the reduced dynamical laws agree qualitatively and/or quantitatively as well as fail to agree with those from GLE on vortex interaction.

The paper is organized as follows. In Section 2, we briefly review the reduced dynamical laws of vortex interaction of the GLE (1.1) with either Dirichlet or homogeneous Neumann BC and present numerical methods to discretize them. In Section 3, efficient and accurate numerical methods are presented for discretizing the GLE in a rectangle or a disk with different BCs. In Section 4, numerical results are reported for vortex interaction of GLE under Dirichlet BC, and similar results for GLE under homogeneous Neumann BC are reported in Section 5. Finally, some conclusions are drawn in Section 6.

2 Reduced dynamical laws and their discretization

In this section, we review two different forms of the reduced dynamical laws for dynamics of vortex centers in the GLE (1.1) with either Dirichlet or homogeneous Neumann BC, show their equivalence and present efficient numerical methods to discretize them.

We assume that, in the initial data ψ_0^ε, there are exactly M isolated and distinct vortices whose centers are located at $\mathbf{x}_1^0=(x_1^0,y_1^0)$, $\mathbf{x}_2^0=(x_2^0,y_2^0)$, $\cdots$, $\mathbf{x}_M^0=(x_M^0,y_M^0)$ with winding numbers n_1, n_2, $\cdots$, n_M, respectively. The winding number of each vortex can be chosen as either 1 or -1, i.e. $n_j=1$ or -1 for $j=1,2,\cdots,M$. At time $t\geq 0$, the M isolated and distinct vortex centers are located at $\mathbf{x}_1(t)=(x_1(t),y_1(t))$, $\mathbf{x}_2(t)=(x_2(t),y_2(t))$, $\cdots$, and $\mathbf{x}_M(t)=(x_M(t),y_M(t))$. Denote

$$X^0:=(\mathbf{x}_1^0,\mathbf{x}_2^0,\cdots,\mathbf{x}_M^0),\qquad X:=X(t)=(\mathbf{x}_1(t),\mathbf{x}_2(t),\cdots,\mathbf{x}_M(t)),\qquad t\geq 0,$$

then the renormalized energy associated to the M vortex centers is defined as [7,23]

$$W(X):=W(X(t))=-\sum_{1\leq j\neq l\leq M} n_j n_l \ln\left|\mathbf{x}_j(t)-\mathbf{x}_l(t)\right|,\qquad t\geq 0. \tag{2.1}$$

2.1 Under the Dirichlet BC

For the GLE (1.1) with Dirichlet BC (1.3), when $\varepsilon\to 0$, two different forms of reduced dynamical laws have been obtained in the literatures for governing the motion of the M vortex centers.

The first one which is widely used has been derived formally and rigorously in the literature, see for instance [7,9,12,25,33] and references therein:

$$\frac{d}{dt}\mathbf{x}_j(t)=-\nabla_{\mathbf{x}_j}[W(X)+W_{\rm dbc}(X)],\qquad j=1,\cdots,M,\quad t>0, \tag{2.2}$$

with initial condition

$$\mathbf{x}_j(0)=\mathbf{x}_j^0,\qquad j=1,2,\cdots,M. \tag{2.3}$$

Here the renormalized energy $W_{\rm dbc}(X)$ comes from the effect of the Dirichlet BC associated to the M vortex centers $X=X(t)$ and it is defined as [7,23]:

$$W_{\rm dbc}(X)=-\sum_{j=1}^{M}n_jR(\mathbf{x}_j;X)+\int_{\partial\Omega}\left[R(\mathbf{x};X)+\sum_{j=1}^{M}n_j\ln|\mathbf{x}-\mathbf{x}_j|\right]\frac{\partial_{\mathbf{n}_\perp}\omega(\mathbf{x})}{2\pi}\,ds, \tag{2.4}$$

where, for any fixed $X\in\Omega^M$, $R(\mathbf{x};X)$ is a harmonic function in $\mathbf{x}$, i.e.

$$\Delta R(\mathbf{x};X)=0, \qquad \mathbf{x}\in\Omega, \tag{2.5}$$

with the following Neumann BC

$$\frac{\partial R(\mathbf{x};X)}{\partial\mathbf{n}}=\partial_{\mathbf{n}_\perp}\omega(\mathbf{x})-\frac{\partial}{\partial\mathbf{n}}\sum_{l=1}^{M}n_l\ln|\mathbf{x}-\mathbf{x}_l|, \qquad \mathbf{x}\in\partial\Omega. \tag{2.6}$$

Using an identity in [7] (see Eq. (51) on page 84),

$$\nabla_{\mathbf{x}_j}[W(X)+W_{\rm dbc}(X)]=-2n_j\nabla_{\mathbf{x}}\left[R(\mathbf{x};X)+\sum_{l=1\&l\neq j}^{M}n_l\ln|\mathbf{x}-\mathbf{x}_l|\right]_{\mathbf{x}=\mathbf{x}_j},$$

the above reduced dynamical law (2.2) can be simplified, for $1\le j\le M$, as

$$\frac{d}{dt}\mathbf{x}_j(t)=2n_j\left[\nabla_{\mathbf{x}}R(\mathbf{x};X)|_{\mathbf{x}=\mathbf{x}_j(t)}+\sum_{l=1\&l\neq j}^{M}n_l\frac{\mathbf{x}_j(t)-\mathbf{x}_l(t)}{|\mathbf{x}_j(t)-\mathbf{x}_l(t)|^2}\right], \qquad t>0. \tag{2.7}$$

The second one which is easier from the computational point of view has been obtained by Jerrard and Soner [15], for $1\le j\le M$, as

$$\frac{d}{dt}\mathbf{x}_j(t)=2n_j\left[J\nabla_{\mathbf{x}}Q(\mathbf{x};X)|_{\mathbf{x}=\mathbf{x}_j(t)}+\sum_{l=1\&l\neq j}^{M}n_l\frac{\mathbf{x}_j(t)-\mathbf{x}_l(t)}{|\mathbf{x}_j(t)-\mathbf{x}_l(t)|^2}\right], \qquad t>0; \tag{2.8}$$

where J is a 2×2 symplectic matrix defined as

$$J=\begin{pmatrix}0 & 1\\ -1 & 0\end{pmatrix},$$

and for any fixed $X\in\Omega^M$, $Q(\mathbf{x};X)$ is a harmonic function in $\mathbf{x}$ and satisfies the following Dirichlet BC

$$Q(\mathbf{x};X)=\omega(\mathbf{x})-\sum_{l=1}^{M}n_l\theta(\mathbf{x}-\mathbf{x}_l), \qquad \mathbf{x}\in\partial\Omega, \tag{2.9}$$

with the function $\theta\colon\mathbb{R}^2\to[0,2\pi)$ defined as

$$\cos(\theta(\mathbf{x}))=\frac{x}{|\mathbf{x}|}, \qquad \sin(\theta(\mathbf{x}))=\frac{y}{|\mathbf{x}|}, \qquad 0\neq\mathbf{x}=(x,y)\in\mathbb{R}^2. \tag{2.10}$$

In the above two different forms of the reduced dynamical laws for GLE, although the two harmonic functions $R(\mathbf{x};X)$ and $Q(\mathbf{x};X)$ satisfy different BCs, the two different forms of the reduced dynamical laws are indeed equivalent.

Lemma 2.1. *For any fixed $X\in\Omega^M$, we have the following identity*

$$\nabla_{\mathbf{x}}R(\mathbf{x};X)=J\nabla_{\mathbf{x}}Q(\mathbf{x};X),\qquad \mathbf{x}\in\Omega, \tag{2.11}$$

which immediately implies the equivalence of the two reduced dynamical laws (2.7) *and* (2.8).

Proof. For any fixed $X\in\Omega^M$, since $\nabla\cdot(J\nabla_{\mathbf{x}}Q(\mathbf{x};X))=\partial_{yx}Q(\mathbf{x};X)-\partial_{xy}Q(\mathbf{x};X)=0$, there exists a function $\varphi(\mathbf{x})$ such that

$$J\nabla_{\mathbf{x}}Q(\mathbf{x};X)=\nabla\varphi(\mathbf{x}),\qquad \mathbf{x}\in\Omega.$$

Thus, $\varphi(\mathbf{x})$ satisfies the Laplace equation

$$\Delta\varphi(\mathbf{x})=\nabla\cdot(J\nabla_{\mathbf{x}}Q(\mathbf{x};X))=\partial_{yx}\varphi(\mathbf{x})-\partial_{xy}\varphi(\mathbf{x})=0,\qquad \mathbf{x}\in\Omega, \tag{2.12}$$

with the following Neumann BC

$$\partial_{\mathbf{n}}\varphi(\mathbf{x})=(J\nabla_{\mathbf{x}}Q(\mathbf{x};X))\cdot\mathbf{n}=\nabla_{\mathbf{x}}Q(\mathbf{x};X)\cdot\mathbf{n}_{\perp}=\partial_{\mathbf{n}_{\perp}}Q(\mathbf{x};X),\qquad \mathbf{x}\in\partial\Omega. \tag{2.13}$$

Noticing (2.9), we obtain

$$\partial_{\mathbf{n}}\varphi(\mathbf{x})=\partial_{\mathbf{n}_{\perp}}\omega(\mathbf{x})-\frac{\partial}{\partial\mathbf{n}_{\perp}}\sum_{l=1}^{N}n_l\theta(\mathbf{x}-\mathbf{x}_l)=\partial_{\mathbf{n}_{\perp}}\omega(\mathbf{x})-\frac{\partial}{\partial\mathbf{n}}\sum_{l=1}^{N}n_l\ln|\mathbf{x}-\mathbf{x}_l|,\quad \mathbf{x}\in\partial\Omega. \tag{2.14}$$

Combining (2.12), (2.14), (2.5) and (2.6), we get

$$\Delta(R(\mathbf{x};X)-\varphi(\mathbf{x}))=0,\quad \mathbf{x}\in\Omega,\qquad \partial_{\mathbf{n}}(R(\mathbf{x};X)-\varphi(\mathbf{x}))=0,\quad \mathbf{x}\in\partial\Omega. \tag{2.15}$$

Thus

$$R(\mathbf{x};X)=\varphi(\mathbf{x})+\text{constant},\qquad \mathbf{x}\in\Omega,$$

which immediately implies the equality (2.11). □

2.2 Under the homogeneous Neumann BC

Similarly, for the GLE (1.1) with the homogeneous Neumann BC (1.4), when $\varepsilon\to 0$, there are also two different forms of the reduced dynamical laws that govern the motion of the M vortex centers.

Again, by using the renormalized energy W_{nbc} which comes from the effect of the homogeneous Neumann BC associated to the M vortex centers $X=X(t)$

$$W_{\text{nbc}}(X)=-\sum_{j=1}^{M}n_j\tilde{R}(\mathbf{x}_j;X), \tag{2.16}$$

where, for any fixed $X\in\Omega^M$, $\tilde{R}(\mathbf{x};X)$ is a harmonic function in $\mathbf{x}$ and satisfies the following Dirichlet BC

$$\tilde{R}(\mathbf{x};X)=-\sum_{l=1}^{M}n_l\ln|\mathbf{x}-\mathbf{x}_l|,\qquad \mathbf{x}\in\partial\Omega, \tag{2.17}$$

the first one has been derived formally and rigorously by many authors in the literatures [9, 12, 25, 31, 32] as

$$\frac{d}{dt}\mathbf{x}_j(t) = -\nabla_{\mathbf{x}_j}[W(X)+W_{\rm nbc}(X)], \qquad j=1,\cdots,M, \quad t>0. \tag{2.18}$$

Using the following identity

$$\nabla_{\mathbf{x}_j}[W(X)+W_{\rm nbc}(X)] = -2n_j\nabla_{\mathbf{x}}\left[\tilde{R}(\mathbf{x};X)+\sum_{l=1\&l\neq j}^{M} n_l \ln|\mathbf{x}-\mathbf{x}_l|\right]_{\mathbf{x}_j}, \tag{2.19}$$

the above reduced dynamical laws collapse, for $1\le j\le M$, as

$$\frac{d}{dt}\mathbf{x}_j(t) = 2n_j\left[\nabla_{\mathbf{x}}\tilde{R}(\mathbf{x};X)|_{\mathbf{x}=\mathbf{x}_j(t)}+\sum_{l=1\&l\neq j}^{M} n_l\frac{\mathbf{x}_j(t)-\mathbf{x}_l(t)}{|\mathbf{x}_j(t)-\mathbf{x}_l(t)|^2}\right], \qquad t>0. \tag{2.20}$$

Similarly, the second one in this case has been obtained by Jimbo and Morita [19–21], for $1\le j\le M$, as

$$\frac{d}{dt}\mathbf{x}_j(t) = 2n_j\left[J\nabla_{\mathbf{x}}\tilde{Q}(\mathbf{x};X)|_{\mathbf{x}=\mathbf{x}_j(t)}+\sum_{l=1\&l\neq j}^{M} n_l\frac{\mathbf{x}_j(t)-\mathbf{x}_l(t)}{|\mathbf{x}_j(t)-\mathbf{x}_l(t)|^2}\right], \qquad t>0; \tag{2.21}$$

where, for any fixed $X\in\Omega^M$, $\tilde{Q}(\mathbf{x};X)$ is a harmonic function in $\mathbf{x}$ and satisfies the following Neumann BC

$$\frac{\partial\tilde{Q}(\mathbf{x};X)}{\partial\mathbf{n}} = -\frac{\partial}{\partial\mathbf{n}}\sum_{l=1}^{M} n_l\theta(\mathbf{x}-\mathbf{x}_l), \qquad \mathbf{x}\in\partial\Omega. \tag{2.22}$$

Similar to the proof of Lemma 2.1, we can establish the equivalence of the above two different forms of the reduced dynamical laws for the GLE under homogeneous Neumann BC.

Lemma 2.2. *The reduced dynamical laws* (2.20) *and* (2.21) *are equivalent.*

In order to compare the solution of the reduced dynamical laws (2.7) or (2.8) and (2.20) or (2.21) with those from the GLE under Dirichlet or homogeneous Neumann BC, respectively, the ODEs (2.7) or (2.8) and (2.20) or (2.21) are discretized by the standard fourth order Runge-Kutta method. For each fixed $X\in\Omega^M$, when the domain Ω is a rectangle, the Laplace equation (2.5) with BCs (2.6) or (2.17) or (2.9) or (2.22) is discretized by the standard second order finite difference method; and respectively, when the domain Ω is a disk, they are discretized in θ-direction via the Fourier pseudospectral method and in r-direction via the finite element method (FEM) with (r,θ) the polar coordinates. For details, one can see similar discretizations in subsections 3.2 & 3.3 below and we omit them here for brevity.

3 Numerical methods

In this section, we present efficient and accurate numerical methods for discretizing the GLE (1.1) on either a rectangle or a disk with initial condition (1.2) and under either Dirichlet or homogeneous Neumann BC. The key ideas in our numerical methods are based on: (i) applying a time-splitting technique which has been widely used for nonlinear partial differential equations [13,35] to decouple the nonlinearity in the GLE; and (ii) adapt proper finite difference and/or spectral method to discretize a gradient flow with constant coefficient.

3.1 Time-splitting

Let $\tau := \triangle t > 0$ be the time step size, denote $t_n = n\tau$ for $n \geq 0$. For $n = 0,1,\cdots$, from time $t = t_n$ to $t = t_{n+1}$, the GLE (1.1) is solved in two splitting steps. One first solves

$$\lambda_\varepsilon \partial_t \psi^\varepsilon(\mathbf{x},t) = \frac{1}{\varepsilon^2}(1-|\psi^\varepsilon|^2)\psi^\varepsilon, \qquad \mathbf{x}\in\Omega, \quad t \geq t_n, \tag{3.1}$$

for the time step of length τ, followed by solving

$$\lambda_\varepsilon \partial_t \psi^\varepsilon(\mathbf{x},t) = \Delta \psi^\varepsilon, \qquad \mathbf{x}\in\Omega, \quad t \geq t_n, \tag{3.2}$$

for the same time step. Eq. (3.2) is discretized in the next two subsections on a rectangle and a disk, respectively. For $t \in [t_n, t_{n+1}]$, we easily obtain the following ODE for $\rho(\mathbf{x},t) = |\psi^\varepsilon(\mathbf{x},t)|^2$:

$$\partial_t \rho(\mathbf{x},t) = \frac{2}{\varepsilon^2\lambda_\varepsilon}[1-\rho(\mathbf{x},t)]\rho(\mathbf{x},t), \qquad \mathbf{x}\in\Omega, \quad t_n \leq t \leq t_{n+1}. \tag{3.3}$$

Solving the above ODE, we get

$$\rho(\mathbf{x},t) = \frac{\rho(\mathbf{x},t_n)}{\rho(\mathbf{x},t_n)+(1-\rho(\mathbf{x},t_n))\exp[-\frac{2}{\varepsilon^2\lambda_\varepsilon}(t-t_n)]}. \tag{3.4}$$

Plugging (3.4) into (3.1), we can integrate it exactly to get

$$\psi^\varepsilon(\mathbf{x},t) = \frac{\psi^\varepsilon(\mathbf{x},t_n)}{\sqrt{|\psi^\varepsilon(\mathbf{x},t_n)|^2+(1-|\psi^\varepsilon(\mathbf{x},t_n)|^2)\exp(-\frac{2}{\varepsilon^2\lambda_\varepsilon}(t-t_n))}}. \tag{3.5}$$

We remark here that, in practice, we always use the second-order Strang splitting [35], that is, from time $t = t_n$ to $t = t_{n+1}$: (i) evolve (3.1) for half time step $\tau/2$ with initial data given at $t = t_n$; (ii) evolve (3.2) for one step τ starting with the new data; and (iii) evolve (3.1) for half time step $\tau/2$ again with the newer data.

3.2 Discretization when Ω is a rectangle

Let $\Omega=[a,b]\times[c,d]$ be a rectangular domain, and denote mesh sizes $h_x=\frac{b-a}{N}$ and $h_y=\frac{d-c}{L}$ with N and L being two even positive integers.

Firstly, we present a Crank-Nicolson 4th-order compact finite difference (CNFD) method for discretizing Eq. (3.2) with Dirichlet BC (1.3) by using the 4th-order compact finite difference discretization for spatial derivatives followed by a Crank-Nicolson scheme for temporal derivative. To this end, for $j=0,1,\cdots,N$, $l=0,1,\cdots,L$ and $n\geq 0$, we denote (x_j,y_l) with $x_j=a+jh_x$ and $y_l=c+lh_y$ as the grid points, and let $\psi_{j,l}^{\varepsilon,n}$ be the numerical approximation of $\psi^\varepsilon(x_j,y_l,t_n)$. Moreover, we define the finite difference operators as

$$\delta_x^2\psi_{j,l}^{\varepsilon,n}=\frac{\psi_{j+1,l}^{\varepsilon,n}-2\psi_{j,l}^{\varepsilon,n}+\psi_{j-1,l}^{\varepsilon,n}}{h_x^2},\qquad \delta_y^2\psi_{j,l}^{\varepsilon,n}=\frac{\psi_{j,l+1}^{\varepsilon,n}-2\psi_{j,l}^{\varepsilon,n}+\psi_{j,l-1}^{\varepsilon,n}}{h_y^2},$$

then a CNFD discretization for (3.2) reads, i.e. for $1\leq j\leq N-1$ and $1\leq l\leq L-1$

$$\frac{\lambda_\varepsilon}{\tau}\left[I+\frac{h_x^2}{12}\delta_x^2+\frac{h_y^2}{12}\delta_y^2\right]\left(\psi_{j,l}^{\varepsilon,n+1}-\psi_{j,l}^{\varepsilon,n}\right)=\left[\delta_x^2+\delta_y^2+\frac{h_x^2+h_y^2}{12}\delta_x^2\delta_y^2\right]\left(\frac{\psi_{j,l}^{\varepsilon,n+1}+\psi_{j,l}^{\varepsilon,n}}{2}\right),\tag{3.6}$$

where I is the identity operator and the BC (1.3) is discretized as

$$\begin{aligned}&\psi_{0,l}^{\varepsilon,n+1}=g(a,y_l),\qquad \psi_{N,l}^{\varepsilon,n+1}=g(b,y_l),\qquad l=0,1,\cdots,L,\\&\psi_{j,0}^{\varepsilon,n+1}=g(x_j,c),\qquad \psi_{j,L}^{\varepsilon,n+1}=g(x_j,d),\qquad j=0,1,\cdots,N.\end{aligned}$$

Here although an implicit time discretization is applied for (3.2), the linear system in (3.6) can be solved explicitly via direct Poisson solver through discrete sine transform (DST) [22] at the computational cost of $\mathcal{O}(NL\ln(NL))$.

Combining the above CNFD discretization with the second order Strang splitting presented in the previous subsection, we obtain a time-splitting Crank-Nicolson finite difference (TSCNFD) discretization for the GLE (1.1) on a rectangle with Dirichlet BC (1.3). This TSCNFD discretization is unconditionally stable, second order in time and fourth order in space, the memory cost is $\mathcal{O}(NL)$ and the computational cost per time step is $\mathcal{O}(NL\ln(NL))$.

Secondly, we present a cosine pseudospectral method for Eq. (3.2) with homogeneous Neumann BC (1.4) by using cosine spectral discretization for spatial derivatives followed by integrating in time *exactly*. To this end, let

$$Y_{NL}=\text{span}\left\{\phi_{pq}(\mathbf{x})=\cos(\mu_p^x(x-a))\cos(\mu_q^y(y-c)),\ 0\leq p\leq N-1,\ 0\leq q\leq L-1\right\},$$

with

$$\mu_p^x=\frac{p\pi}{b-a},\quad p=0,1,\cdots,N-1;\qquad \mu_q^y=\frac{q\pi}{d-c},\quad q=0,1,\cdots,L-1,$$

then the cosine spectral discretization for (3.2) with (1.4) is as follows: Find $\psi^{\varepsilon}_{NL}(\mathbf{x},t)\in Y_{NL}$, i.e.

$$\psi^{\varepsilon}_{NL}(\mathbf{x},t)=\sum_{p=0}^{N-1}\sum_{q=0}^{L-1}\hat{\psi}^{\varepsilon}_{pq}(t)\phi_{pq}(\mathbf{x}),\qquad \mathbf{x}\in\Omega,\quad t\geq t_n, \tag{3.7}$$

such that

$$\lambda_{\varepsilon}\partial_t\psi^{\varepsilon}_{NL}(\mathbf{x},t)=\Delta\psi^{\varepsilon}_{NL}(\mathbf{x},t),\qquad \mathbf{x}\in\Omega,\quad t\geq t_n. \tag{3.8}$$

Plugging (3.7) into (3.8), noticing the orthogonality of the cosine functions, for $0\leq p\leq N-1$ and $0\leq q\leq L-1$, we find

$$\lambda_{\varepsilon}\frac{d}{dt}\hat{\psi}^{\varepsilon}_{pq}(t)=-\left[(\mu^x_p)^2+(\mu^y_q)^2\right]\hat{\psi}^{\varepsilon}_{pq}(t),\qquad t\geq t_n. \tag{3.9}$$

The above ODE can be integrated *exactly* in time, i.e.

$$\hat{\psi}^{\varepsilon}_{pq}(t_{n+1})=e^{-\left[(\mu^x_p)^2+(\mu^y_q)^2\right]\tau/\lambda_{\varepsilon}}\hat{\psi}^{\varepsilon}_{pq}(t_n),\qquad 0\leq p\leq N-1,\quad 0\leq q\leq L-1. \tag{3.10}$$

However, the above procedure is not suitable in practice due to the difficulty of computing the integrals in (3.7). In practice, we need to approximate the integrals by a quadrature rule on grids. For $j=0,1,\cdots,N-1$, $l=0,1,\cdots,L-1$ and $n\geq 0$, we denote (x_j,y_l) with $x_{j+\frac{1}{2}}=a+(j+\frac{1}{2})h_x$ and $y_{l+\frac{1}{2}}=c+(l+\frac{1}{2})h_y$ as the grid points, and let $\psi^{\varepsilon,n}_{j+\frac{1}{2},l+\frac{1}{2}}$ be the numerical approximation of $\psi^{\varepsilon}(x_{j+\frac{1}{2}},y_{l+\frac{1}{2}},t_n)$, then, by choosing $\psi^{\varepsilon,0}_{j+\frac{1}{2},l+\frac{1}{2}}=\psi^{\varepsilon}_0(x_{j+\frac{1}{2}},y_{l+\frac{1}{2}})$, a cosine pseudospectral approximation for (3.2) with (1.4) reads as:

$$\psi^{\varepsilon,n+1}_{j+\frac{1}{2},l+\frac{1}{2}}=\sum_{p=0}^{N-1}\sum_{q=0}^{L-1}\alpha^x_p\alpha^y_q e^{-\left[(\mu^x_p)^2+(\mu^y_q)^2\right]\tau/\lambda_{\varepsilon}}\hat{\psi}^{\varepsilon,n}_{pq}\phi_{pq}(x_{j+\frac{1}{2}},y_{l+\frac{1}{2}}),\qquad n\geq 0, \tag{3.11}$$

where

$$\hat{\psi}^{\varepsilon,n}_{p,q}=\alpha^x_p\alpha^y_q\sum_{j=0}^{N-1}\sum_{l=0}^{L-1}\psi^{\varepsilon,n}_{j+\frac{1}{2},l+\frac{1}{2}}\phi_{pq}(x_{j+\frac{1}{2}},y_{l+\frac{1}{2}}),\qquad 0\leq p\leq N-1,\quad 0\leq q\leq L-1,$$

with

$$\alpha^x_p=\begin{cases}\sqrt{\frac{1}{N}}, & p=0,\\ \sqrt{\frac{2}{N}}, & 1\leq p\leq N-1,\end{cases}\qquad \alpha^y_q=\begin{cases}\sqrt{\frac{1}{L}}, & q=0,\\ \sqrt{\frac{2}{L}}, & 1\leq q\leq L-1.\end{cases}$$

Again, combining the above cosine pseudospectral discretization with the second order Strang splitting presented in Subsection 3.1, we obtain a time-splitting cosine pseudospectral (TSCP) discretization for the GLE (1.1) on a rectangle with homogeneous Neumann BC (1.4). This TSCP discretization is unconditionally stable, second order in time and spectral order in space, the memory cost is $\mathcal{O}(NL)$ and the computational cost per time step is $\mathcal{O}(NL\ln(NL))$ via discrete cosine transform (DCT) [34].

Remark 3.1. If the homogeneous Neumann BC (1.4) is replaced by periodic BC, the above TSCP discretization for the GLE (1.1) is still valid provided that we replace the cosine basis functions by the Fourier basis functions in the spectral discretization and use the quadrature rule associated to the Fourier functions [34]. We omit the details here for brevity.

3.3 Discretization when Ω is a disk

Let $\Omega=\{\mathbf{x} \mid |\mathbf{x}|<R\}$ be a disk with $R>0$ a fixed constant. In this case, it is natural to adopt the polar coordinate (r,θ) in our numerical discretization. In order to discretize (3.2) with either (1.3) or (1.4), we apply the standard Fourier pseudospectral method in θ-direction [34], finite element method in r-direction, and Crank-Nicolson method in time [4, 5, 37]. Plugging the following truncated Fourier expansion for ψ^ε

$$\psi^\varepsilon(r,\theta,t)=\sum_{l=-L/2}^{l=L/2-1}\hat{\psi}_l(r,t)e^{il\theta}, \qquad 0\le r\le R, \quad 0\le\theta\le 2\pi, \tag{3.12}$$

with L an even positive number and $\hat{\psi}_l$ the Fourier coefficients for the l-th mode into (3.2) and using the orthogonality of the Fourier functions, we obtain for $l=-\frac{L}{2},\cdots,\frac{L}{2}-1$:

$$\lambda_\varepsilon\partial_t\hat{\psi}_l(r,t)=\frac{1}{r}\partial_r\left(r\partial_r\hat{\psi}_l(r,t)\right)-\frac{l^2}{r^2}\hat{\psi}_l(r,t), \qquad 0<r<R, \quad t\ge t_n, \tag{3.13}$$

with the following BC at $r=0$

$$\partial_r\hat{\psi}_0(0,t)=0, \quad \hat{\psi}_l(0,t)=0, \quad l\neq 0, \quad t\ge t_n. \tag{3.14}$$

When the Dirichlet BC (1.3) is used for (3.2), we then impose the following BC at $r=R$:

$$\hat{\psi}_l(R,t)=\hat{g}_l:=\frac{1}{2\pi}\int_0^{2\pi}g(\theta)e^{-il\theta}d\theta, \qquad -\frac{L}{2}\le l\le\frac{L}{2}-1, \quad t\ge t_n. \tag{3.15}$$

Let P^k denote all polynomials with degree at most k, denote $0=r_0<r_1<\cdots<r_N=R$ be a partition for the interval $[0,R]$ with N a positive integer and a mesh size $h=\max_{0\le j\le N-1}(r_{j+1}-r_j)$, and define a finite element space by

$$U^h=\left\{u^h\in C[0,R] \mid u^h|_{[r_j,r_{j+1}]}\in P^k,\ 0\le j\le N-1\right\}.$$

Introducing the following finite element approximate sets associated to the Dirichlet BCs for $-\frac{L}{2}\le l\le\frac{L}{2}-1$ as

$$U_l^g=\begin{cases}\left\{u^h\in U^h \mid u^h(R)=\hat{g}_0\right\} & l=0,\\ \left\{u^h\in U^h \mid u^h(0)=0,\ u^h(R)=\hat{g}_l\right\} & l\neq 0;\end{cases} \tag{3.16}$$

then we obtain the FEM approximation for (3.13) with (3.14) and (3.15): Find $\hat{\psi}_l^h(\cdot,t)\in U_l^g$ with $-\frac{L}{2}\le l\le\frac{L}{2}-1$ such that

$$\frac{d}{dt}A(\hat{\psi}_l^h,\phi^h)=B(\hat{\psi}_l^h,\phi^h)+l^2C(\hat{\psi}_l^h,\phi^h),\quad \forall\phi^h\in U_l^0,\quad t_n\le t\le t_{n+1};\tag{3.17}$$

where the bilinear forms A, B and C are defined as

$$A(u^h,v^h)=\lambda_\varepsilon\int_0^R ru^hv^hdr,\qquad B(u^h,v^h)=-\int_0^R r\partial_r u^h\partial_r v^h dr,$$
$$C(u^h,v^h)=-\int_0^R\frac{1}{r}u^hv^hdr,\qquad \forall u^h,\,v^h\in U^h.$$

The above ODE system (3.17) is then discretized by the standard Crank-Nicolson scheme in time. Here although an implicit time discretization is applied for (3.17), the one-dimensional nature of the problem makes the coefficient matrix for the linear system band limited. For example, if the piecewise linear polynomial is used, i.e. $k=1$ in U^h, the matrix is tridiagonal. Thus for each fixed $-\frac{L}{2}\le l\le\frac{L}{2}-1$, fast algorithms can be applied to solve the resulting linear systems at the cost of $\mathcal{O}(N)$.

Similarly, when the homogeneous Neumann BC (1.4) is used for (3.2), the above discretization is still valid provided that we replace the BC at $r=R$ in (3.15) by

$$\partial_r\hat{\psi}_l(R,t)=0,\qquad -\frac{L}{2}\le l\le\frac{L}{2}-1,\quad t\ge t_n;\tag{3.18}$$

the finite element subsets U_l^g in (3.16) and U_l^0 in (3.17) by the following finite element spaces

$$U_l^n=\begin{cases}U^h & l=0,\\ \{u^h\in U^h\mid u^h(0)=0\} & l\neq 0.\end{cases}\tag{3.19}$$

The detailed discretization is omitted here for brevity.

Remark 3.2. Eq. (3.13) with (3.14) can also be discretized in space by either finite difference or Legendre or Chebyshev pseudospectral method [34] and in time by the Crank-Nicolson method.

4 Numerical results under Dirichlet BC

In this section, we report numerical results for vortex interactions of GLE (1.1) under the Dirichlet BC (1.3) and compare them with those obtained from the reduced dynamical laws (2.7) with (2.3). For a given bounded domain Ω, the GLE (1.1) is unchanged by the re-scaling $\mathbf{x}\to d\mathbf{x}$, $t\to d^2t$ and $\varepsilon\to d\varepsilon$ with d the diameter of Ω. Thus without lose of generality, in this section and the next, without specification, we always assume that the diameter of Ω is $\mathcal{O}(1)$ and study how the dimensionless parameter ε, initial setup,

boundary value and geometry of the domain Ω affect the dynamics and interaction of vortices. The function g in the Dirichlet BC (1.3) is given as

$$g(\mathbf{x}) = e^{i(h(\mathbf{x})+\sum_{j=1}^{M} n_j \theta(\mathbf{x}-\mathbf{x}_j^0))}, \qquad \mathbf{x}\in\partial\Omega,$$

and the initial condition ψ_0^ε in (1.2) is chosen as

$$\psi_0^\varepsilon(\mathbf{x}) = \psi_0^\varepsilon(x,y) = e^{ih(\mathbf{x})}\prod_{j=1}^{M}\phi_{n_j}^\varepsilon(\mathbf{x}-\mathbf{x}_j^0), \qquad \mathbf{x}=(x,y)\in\bar{\Omega}, \tag{4.1}$$

where $M>0$ is the total number of vortices in the initial data, $h(\mathbf{x})$ is a harmonic function, $\theta(\mathbf{x})$ is defined in (2.10) and for $j=1,2,\cdots,M$, $n_j=1$ or -1, and $\mathbf{x}_j^0=(x_j^0,y_j^0)\in\Omega$ are the winding number and initial location of the j-th vortex, respectively,

$$\phi_{n_j}^\varepsilon(\mathbf{x}) = f^\varepsilon(|\mathbf{x}|)\, e^{in_j\theta(\mathbf{x})}, \qquad \mathbf{x}=(x,y)\in\Omega.$$

Here, $f^\varepsilon(r)$ is chosen as

$$f^\varepsilon(r) = \begin{cases} 1, & r\geq R_0=0.25, \\ f_{\rm v}^\varepsilon(r), & 0\leq r\leq R_0; \end{cases} \tag{4.2}$$

where $f_{\rm v}^\varepsilon$ is the solution of the following problem:

$$\left[\frac{1}{r}\frac{d}{dr}\left(r\frac{d}{dr}\right)-\frac{1}{r^2}+\frac{1}{\varepsilon^2}\left(1-(f_{\rm v}^\varepsilon(r))^2\right)\right]f_{\rm v}^\varepsilon(r)=0, \qquad 0<r<R_0,$$

with the Dirichlet BC

$$f_{\rm v}^\varepsilon(r=0)=0, \qquad f_{\rm v}^\varepsilon(r=R_0)=1.$$

The solution $f_{\rm v}^\varepsilon$ of the above problem is computed numerically and we depict the function $f^\varepsilon(r)$ in Fig. 1 with different ε.

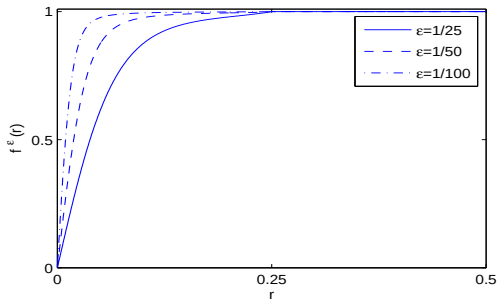

Figure 1: Plot of the function $f^\varepsilon(r)$ in (4.2) with different ε.

To simplify our presentation, for $j=1,2,\cdots,M$, hereafter we let $\mathbf{x}_j^\varepsilon(t)$ and $\mathbf{x}_j^{\rm r}(t)$ be the j-th vortex center in the GLE dynamics and corresponding reduced dynamics, respectively, and denote $d_j^\varepsilon(t)=|\mathbf{x}_j^\varepsilon(t)-\mathbf{x}_j^{\rm r}(t)|$ as their difference. Moreover, in the presentation

of figures, the initial location of a vortex with winding number $+1$, -1 and the location that two vortices merge are marked as '+', '$\circ$' and '$\diamond$', respectively. Finally, in our computations, if not specified, we take $\Omega=[-1,1]^2$ in (1.1), mesh sizes $h_x=h_y=\frac{\varepsilon}{10}$ and time step $\tau=10^{-6}$. The GLE (1.1) with (1.3), (1.2) and (4.1) is solved by the method TSCNFD presented in Section 3.

4.1 Single vortex

Here we present numerical results of the motion of a single quantized vortex in the GLE (1.1) dynamics and its corresponding reduced dynamics, i.e. we take $M=1$, $n_1=1$ and consider following cases: case I. $\mathbf{x}_1^0=(0,0)$, $h(\mathbf{x})=x+y$; case II. $\mathbf{x}_1^0=(0,0)$, $h(\mathbf{x})=x-y$; case III. $\mathbf{x}_1^0=(0,0)$, $h(\mathbf{x})=x^2-y^2$; case IV. $\mathbf{x}_1^0=(0.1,0.2)$, $h(\mathbf{x})=x+y$; case V. $\mathbf{x}_1^0=(0.1,0.2)$, $h(\mathbf{x})=x-y$; and case VI. $\mathbf{x}_1^0=(0.1,0.2)$, $h(\mathbf{x})=x^2-y^2$. Fig. 2 depicts trajectory of the vortex center when $\varepsilon=\frac{1}{32}$ in (1.1) for above 6 cases and d_1^ε with different ε for case II, IV and VI.

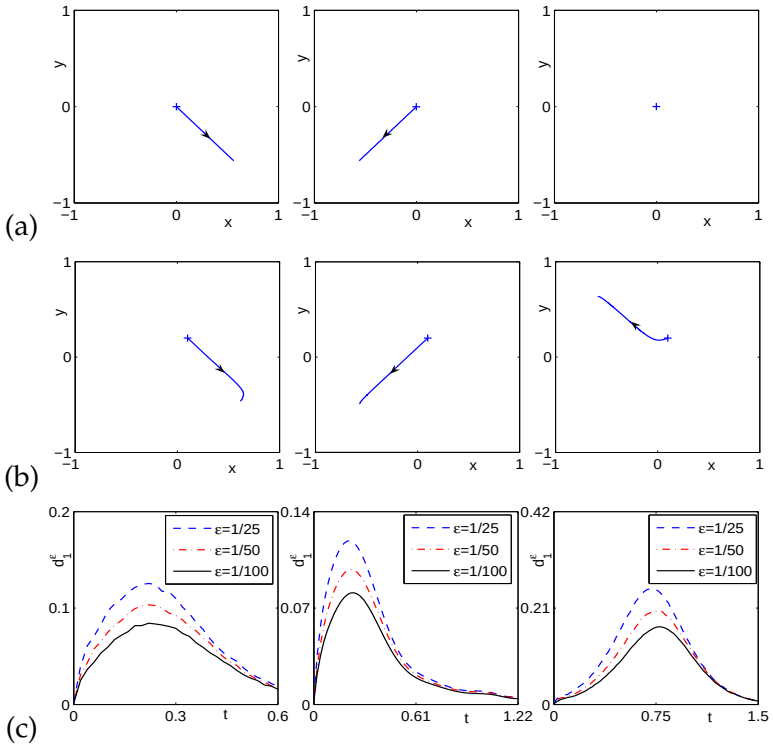

Figure 2: (a)-(b): Trajectory of the vortex center in GLE under Dirichlet BC when $\varepsilon=\frac{1}{32}$ for cases I-VI (from left to right and then from top to bottom), and (c): d_1^ε for different ε for cases II, IV and VI (from left to right) in Section 4.1.

From Fig. 2 and additional numerical experiments not shown here for brevity, we can draw following conclusions: (i). When $h(\mathbf{x})\equiv 0$, the vortex center doesn't move and this

is similar to the case in the whole space. (ii). When $h(\mathbf{x})=(x-by)(x-\frac{y}{b})$ with $b\neq 0$, the vortex does not move if $\mathbf{x}_0=(0,0)$, while it does move if $\mathbf{x}_0\neq(0,0)$ (cf. case III and VI for $b=1$). (iii). When $h(\mathbf{x})\neq 0$ and $h(\mathbf{x})\neq(x-by)(x-\frac{y}{b})$ with $b\neq 0$, in general, the vortex center does move to a different point from its initial location and stays there forever. This is quite different from the situation in the whole space, where a single vortex may move to infinity under the initial data (4.1) with $h(\mathbf{x})\neq 0$ and $\Omega=\mathbb{R}^2$. (iv). In general, the initial location, the geometry of the domain and the boundary value will all affect the motion of the vortex center. (v). When $\varepsilon\to 0$, the dynamics of the vortex center in the GLE dynamics converges uniformly in time to that in the reduced dynamics (cf. Fig. 2) which verifies numerically the validation of the reduced dynamical laws. In fact, based on our extensive numerical experiments, the motion of the vortex center from the reduced dynamical laws agree with those from the GLE dynamics qualitatively when $0<\varepsilon<1$ and quantitatively when $0<\varepsilon\ll 1$.

4.2 Vortex pair

Here we present numerical results of the interaction of vortex pair under the GLE (1.1) dynamics and its corresponding reduced dynamical laws, i.e. we take $M=2$, $n_1=n_2=1$, $\mathbf{x}_1^0=(-0.5,0)$ and $\mathbf{x}_2^0=(0.5,0)$ in (4.1). Fig. 3 depicts time evolution of the amplitude $|\psi^\varepsilon|$, while Fig. 4 shows that of the GL functionals as well as the trajectory of the vortex centers when $\varepsilon=\frac{1}{32}$ in (1.1) with different $h(\mathbf{x})$ in (4.1). Fig. 5 shows time evolution of $\mathbf{x}_1^r(t)$, $\mathbf{x}_1^\varepsilon(t)$ and $d_1^\varepsilon(t)$ with different $h(\mathbf{x})$ in (4.1).

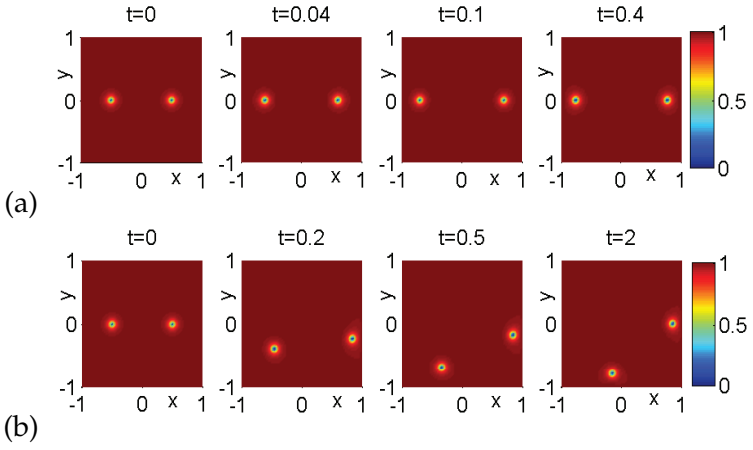

(a)

(b)

Figure 3: Contour plots of $|\psi^\varepsilon(\mathbf{x},t)|$ at different times for the interaction of vortex pair in GLE under Dirichlet BC with $\varepsilon=\frac{1}{32}$ and different $h(\mathbf{x})$ in (4.1): (a) $h(\mathbf{x})=0$, (b) $h(\mathbf{x})=x+y$.

From Figs. 3, 4 & 5 and additional numerical results not shown here for brevity, we can draw the following conclusions for the interaction of vortex pair under the GLE dynamics (1.1) with Dirichlet BC: (i). The two vortices undergo a repulsive interaction, they never collide, both of them move towards the boundary of Ω for a while and finally

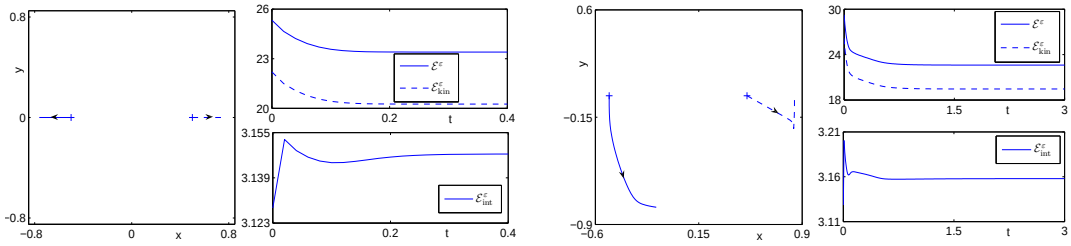

Figure 4: Trajectory of vortex centers (1st and 3rd) and time evolution of the GL functionals (2nd and 4th) for the interaction of vortex pair in GLE under Dirichlet BC with $\varepsilon=\frac{1}{32}$ for different $h(\mathbf{x})$ in (4.1): $h(\mathbf{x})=0$ (left two), $h(\mathbf{x})=x+y$ (right two).

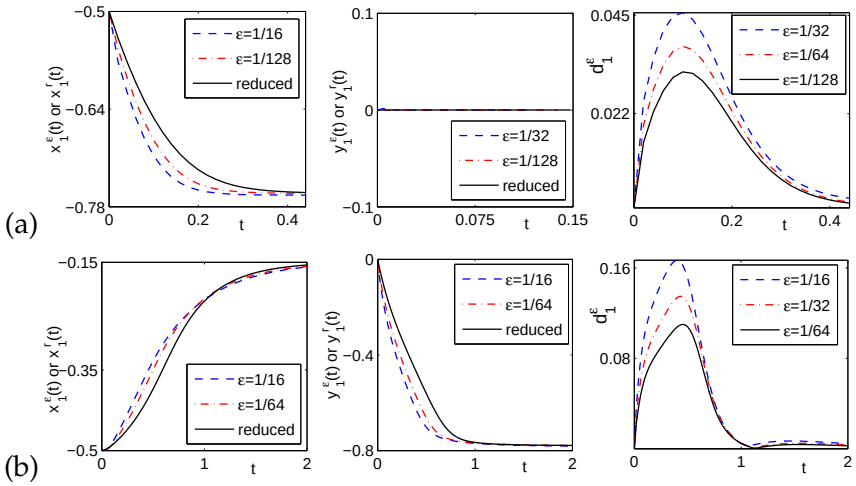

Figure 5: Time evolution of $\mathbf{x}_1^\varepsilon(t)$ and $\mathbf{x}_1^r(t)$ (left and middle) and their difference d_1^ε (right) for different ε for the interaction of vortex pair in GLE under Dirichlet BC for different $h(\mathbf{x})$ in (4.1): (a) $h(\mathbf{x})=0$, (b) $h(\mathbf{x})=x+y$.

stop somewhere near the boundary which indicate that the boundary imposes a repulsive force on the vortices when t is large enough (cf. Figs. 3 & 4). (ii). When $h(\mathbf{x})\equiv 0$, the two vortex centers move outward along the line connecting them initially, and their trajectories are symmetric i.e. $\mathbf{x}_1^\varepsilon(t)=-\mathbf{x}_2^\varepsilon(t)$, while when $h(\mathbf{x})\neq 0$, it affects the motion of the two vortex centers significantly (cf. Fig. 4). (iii). When $\varepsilon\to 0$, the dynamics of the two vortex centers in the GLE dynamics converges uniformly in time to that in the reduced dynamics (cf. Fig. 5) which verifies numerically the validation of the reduced dynamical laws in this case. In fact, based on our extensive numerical experiments, the motion of the two vortex centers from the reduced dynamical laws agree with those from the GLE dynamics qualitatively when $0<\varepsilon<1$ and quantitatively when $0<\varepsilon\ll 1$. (iv). During the dynamics of GLE, the GL functional and its kinetic part decrease when time increases, its interaction part changes dramatically when t is small, and when $t\to\infty$, all the three quantities converge to constants (cf. Fig. 4), which immediately imply that a steady state solution will be reached when $t\to\infty$.

4.3 Vortex dipole

Here we present numerical results of the interaction of vortex dipole in the GLE (1.1) dynamics and its corresponding reduced dynamics, i.e. we take $M=2$, $n_1=-1$, $n_2=1$, $\mathbf{x}_1^0=(-d_0,0)$ and $\mathbf{x}_2^0=(d_0,0)$ in (4.1). Fig. 6 depicts time evolution of the amplitude $|\psi^\varepsilon|$, while Fig. 7 shows that of the GL functionals as well as the trajectory of the vortex centers when $\varepsilon=\frac{1}{32}$ in (1.1) with different d_0 and $h(\mathbf{x})$ in (4.1). Fig. 8 shows time evolution of $\mathbf{x}_1^r(t)$, $\mathbf{x}_1^\varepsilon(t)$ and $d_1^\varepsilon(t)$ with $d_0=0.5$ for different ε and $h(\mathbf{x})$ in (4.1).

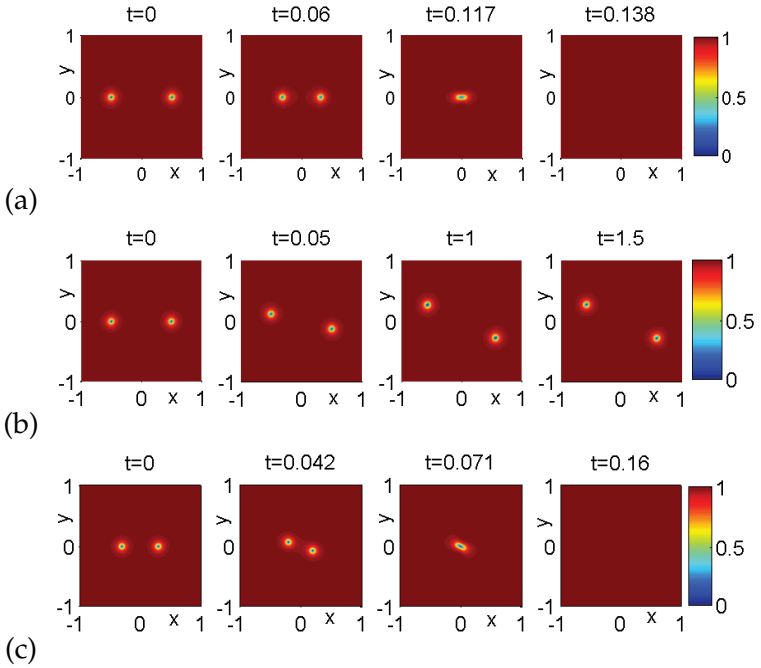

Figure 6: Contour plots of $|\psi^\varepsilon(\mathbf{x},t)|$ at different times for the interaction of vortex dipole in GLE under Dirichlet BC with $\varepsilon=\frac{1}{32}$ for different d_0 and $h(\mathbf{x})$ in (4.1): (a) $h(\mathbf{x})=0$, $d_0=0.5$, (b) $h(\mathbf{x})=x+y$, $d_0=0.5$, (c) $h(\mathbf{x})=x+y$, $d_0=0.3$.

From Figs. 6, 7 & 8 and additional numerical results not shown here for brevity, we can draw the following conclusions for the interaction of vortex dipole under the GLE dynamics (1.1) with Dirichlet BC: (i). Both boundary value, i.e. $h(\mathbf{x})$, and distance between the two vortex centers initially, i.e. $2d_0$, affect the motion of the vortices significantly. (ii). When $h(\mathbf{x})\equiv 0$, for any initial location of the vortex dipole, the two vortices always undergo an attractive interaction and their centers move toward each other along the line connecting them initially, their trajectory are symmetric with respect to the line perpendicular to the segment connecting them initially, and finally, they merge at the middle point of this segment, i.e. the point $\mathbf{x}_{\rm merge}=\frac{1}{2}(\mathbf{x}_1^0+\mathbf{x}_2^0)$ (cf. Figs. 6 & 7). At the collision, both vortices in the vortex dipole merge/annihilate with each other; and after the collision, they will disappear and no vortex is left afterwards during the dynamics.

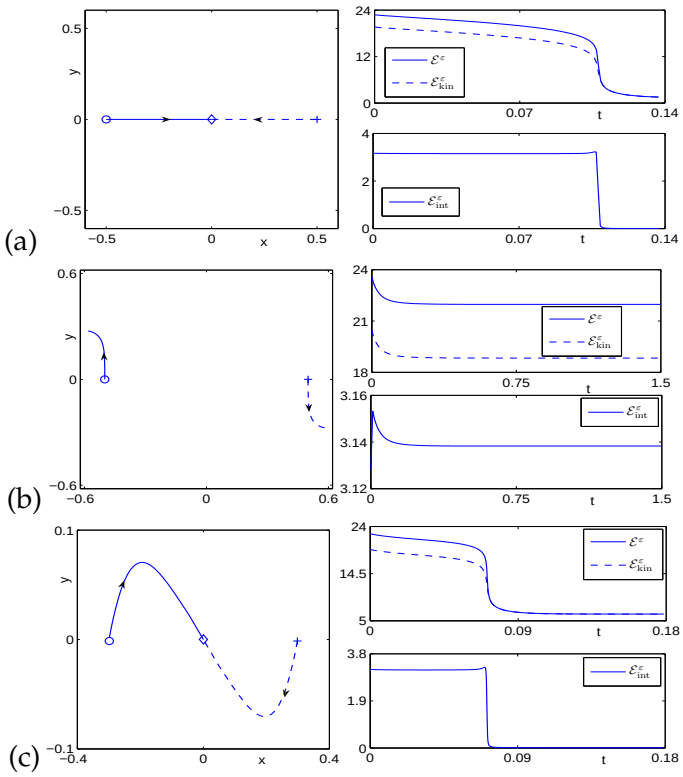

Figure 7: Trajectory of vortex centers (left) and time evolution of the GL functionals (right) for the interaction of vortex dipole in GLE under Dirichlet BC with $\varepsilon=\frac{1}{32}$ for different d_0 and $h(\mathbf{x})$ in (4.1): (a) $h(\mathbf{x})=0$, $d_0=0.5$, (b) $h(\mathbf{x})=x+y$, $d_0=0.5$, (c) $h(\mathbf{x})=x+y$, $d_0=0.3$.

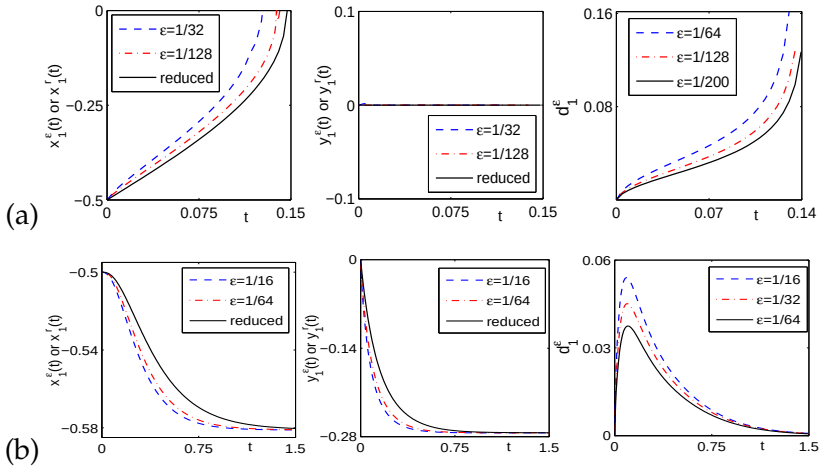

Figure 8: Time evolution of $\mathbf{x}_1^\varepsilon(t)$ and $\mathbf{x}_1^r(t)$ (left and middle) and difference d_1^ε (right) for different ε for the interaction of vortex dipole in GLE under Dirichlet BC with $d_0=0.5$ for different $h(\mathbf{x})$ in (4.1): (a) $h(\mathbf{x})=0$, (b) $h(\mathbf{x})=x+y$.

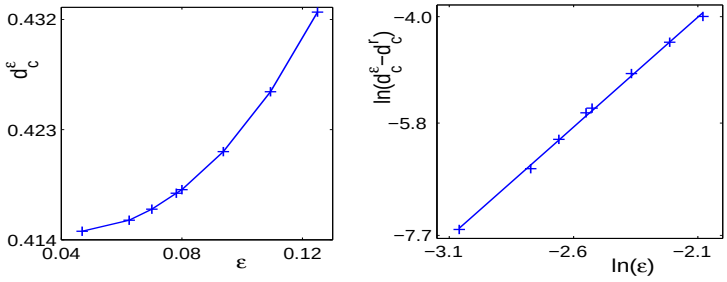

Figure 9: Critical value d_c^ε for the interaction of vortex dipole of the GLE (1.1) under Dirichlet BC with $h(\mathbf{x})\equiv x+y$ in (4.1) for different ε.

For any fixed $0<\varepsilon<1$, there is a collision time T_ε which increases when ε decreases. (iii). When $h(\mathbf{x})=x+y$, the two vortices move along a symmetric trajectory, i.e. $\mathbf{x}_1^\varepsilon(t)=-\mathbf{x}_2^\varepsilon(t)$. Moreover, for the reduced dynamical laws, there exists a critical value d_c^r, which is found numerically as $d_c^r\approx 0.4142$, such that when the distance between the two vortex centers initially $d_0=\frac{1}{2}|\mathbf{x}_1^0-\mathbf{x}_2^0|<d_c^r$, then the vortex dipole will merge at finite time, and respectively, when $d_0>d_c^r$, the vortex dipole will never collide. Similarly, for the vortex dipole under the GLE dynamics, for each fixed $0<\varepsilon<1$, there exists a critical value d_c^ε such that when $d_0<d_c^\varepsilon$, then the vortex dipole will merge at finite time, and respectively, when $d_0>d_c^\varepsilon$, the vortex dipole will never collide (cf. Figs. 6 & 7). We find numerically the critical distance d_c^ε for $0<\varepsilon<1$ and depict them in Fig. 9. From these values, we can fit the following relationship between d_c^ε and d_c^r:

$$d_c^\varepsilon\approx d_c^r+41.26\varepsilon^{3.8},\qquad 0\le\varepsilon<1.$$

(iv). When $\varepsilon\to 0$, the dynamics of the two vortex centers under the GLE dynamics converges uniformly in time to that of the reduced dynamical laws before the collision happens (cf. Fig. 8) which verifies numerically the validation of the reduced dynamical laws in this case. In fact, based on our extensive numerical experiments, the motion of the two vortex centers from the reduced dynamical laws agree with those from the GLE dynamics qualitatively when $0<\varepsilon<1$ and quantitatively when $0<\varepsilon\ll 1$ if the initial distance between the two vortex centers satisfies either $0<d_0<d_c^r$ or $d_0>d_c^\varepsilon$. On the contrary, if $d_c^r<d_0<d_c^\varepsilon$, then the motion of the vortex dipole from the reduced dynamical laws is different qualitatively from that of the GLE dynamics. (v). During the dynamics of GLE, the GL functional decreases when time increases, its kinetic and interaction parts change dramatically when t is small, and when $t\to\infty$, all the three quantities converge to constants (cf. Fig. 7). Moreover, if finite time merging/annihilation happens, the GL functional and its kinetic and interaction parts change significantly during the collision. In addition, when $t\to\infty$, the interaction energy goes to 0 which immediately implies that a steady state will be reached in the form of $\phi^\varepsilon(\mathbf{x})=e^{ic(\mathbf{x})}$, where $c(\mathbf{x})$ is a harmonic function satisfying $c(\mathbf{x})|_{\partial\Omega}=h(\mathbf{x})+\sum_{j=1}^M n_j\theta(\mathbf{x}-\mathbf{x}_j^0)$.

4.4 Vortex lattices

Here we present numerical results of the interaction of vortex lattices under the GLE (1.1) dynamics. We will consider the following cases:

case I. $M=3$, $n_1=n_2=n_3=1$, $\mathbf{x}_1^0=(-0.25,\frac{\sqrt{3}}{4})$, $\mathbf{x}_2^0=(-0.25,-\frac{\sqrt{3}}{4})$, $\mathbf{x}_3^0=(0.5,0)$;

case II. $M=3$, $n_1=n_2=n_3=1$, $\mathbf{x}_1^0=(-0.4,0)$, $\mathbf{x}_2^0=(0,0)$, $\mathbf{x}_3^0=(0.4,0)$;

case III. $M=3$, $n_1=n_2=n_3=1$, $\mathbf{x}_1^0=(0,0.3)$, $\mathbf{x}_2^0=(0.15,0.15)$, $\mathbf{x}_3^0=(0.3,0)$;

case IV. $M=3$, $n_1=-1$, $n_2=n_3=1$, $\mathbf{x}_1^0=(-0.25,\frac{\sqrt{3}}{4})$, $\mathbf{x}_2^0=(-0.25,-\frac{\sqrt{3}}{4})$, $\mathbf{x}_3^0=(0.5,0)$;

case V. $M=3$, $n_2=-1$, $n_1=n_3=1$, $\mathbf{x}_1^0=(-0.4,0)$, $\mathbf{x}_2^0=(0,0)$, $\mathbf{x}_3^0=(0.4,0)$;

case VI. $M=3$, $n_1=-1$, $n_2=n_3=1$, $\mathbf{x}_1^0=(0.2,0.3)$, $\mathbf{x}_2^0=(-0.3,0.4)$, $\mathbf{x}_3^0=(-0.4,-0.2)$;

case VII. $M=4$, $n_1=n_2=n_3=n_4=1$, $\mathbf{x}_1^0=(0,0.5)$, $\mathbf{x}_2^0=(-0.5,0)$, $\mathbf{x}_3^0=(0,-0.5)$, $\mathbf{x}_4^0=(0.5,0)$;

case VIII. $M=4$, $n_1=n_3=-1$, $n_2=n_4=1$, $\mathbf{x}_1^0=(0,0.5)$, $\mathbf{x}_2^0=(-0.5,0)$, $\mathbf{x}_3^0=(0,-0.5)$, $\mathbf{x}_4^0=(0.5,0)$;

case IX. $M=4$, $n_1=n_2=-1$, $n_3=n_4=1$, $\mathbf{x}_1^0=(0,0.5)$, $\mathbf{x}_2^0=(-0.5,0)$, $\mathbf{x}_3^0=(0,-0.5)$, $\mathbf{x}_4^0=(0.5,0)$.

Fig. 10 shows trajectory of the vortex centers when $\varepsilon=\frac{1}{32}$ in (1.1) and $h(\mathbf{x})=0$ in (4.1) for the above 9 cases. From Fig. 10 and additional numerical experiments not shown here for brevity, we can draw the following conclusions: (i) The interaction of vortex lattices under the GLE dynamics with Dirichlet BC is very interesting and complicated. The detailed dynamics and interaction pattern of a lattice depends on its initial alignment of the lattice, geometry of the domain Ω and the boundary value $g(\mathbf{x})$. (ii) For a lattice of M vortices, if they have the same index, no collision will happen for any time $t\geq 0$. On the other hand, if they have opposite index, e.g. $M^+>0$ vortices with index '$+1$' and $M^->0$ vortices with index '-1' satisfying $M^++M^-=M$, collision will always happen at finite time. In addition, when t is sufficiently large, there exist exactly $|M^+-M^-|$ vortices of winding number '$+1$' if $M^+>M^-$, and resp. '-1' if $M^+<M^-$, left in the domain.

4.5 Steady state patterns of vortex lattices with the same index

Here we present the steady state patterns of vortex lattices in the GLE dynamics (1.1) under Dirichlet BC. We study how the geometry of the domain Ω and boundary condition, i.e. $h(\mathbf{x})$, affect the alignment of vortices in the steady states. To this end, we take $\varepsilon=\frac{1}{16}$ in (1.1),

$$n_j=1, \qquad \mathbf{x}_j^0=0.5\left(\cos\left(\frac{2j\pi}{M}\right),\sin\left(\frac{2j\pi}{M}\right)\right), \qquad j=1,2,\cdots,M,$$

i.e., initially we have M like vortices which are located uniformly in a circle centered at origin with radius $R_1=0.5$.

Denote $\phi^\varepsilon(\mathbf{x})$ as the steady state, i.e. $\phi^\varepsilon(\mathbf{x})=\lim_{t\to\infty}\psi^\varepsilon(\mathbf{x},t)$ for $\mathbf{x}\in\Omega$. Fig. 11 depicts the contour plots of the amplitude $|\phi^\varepsilon|$ of the steady state in the GLE dynamics with $h(\mathbf{x})=x^2-y^2+2xy$ in (4.1) for different M and domains, while Fig. 12 depicts similar

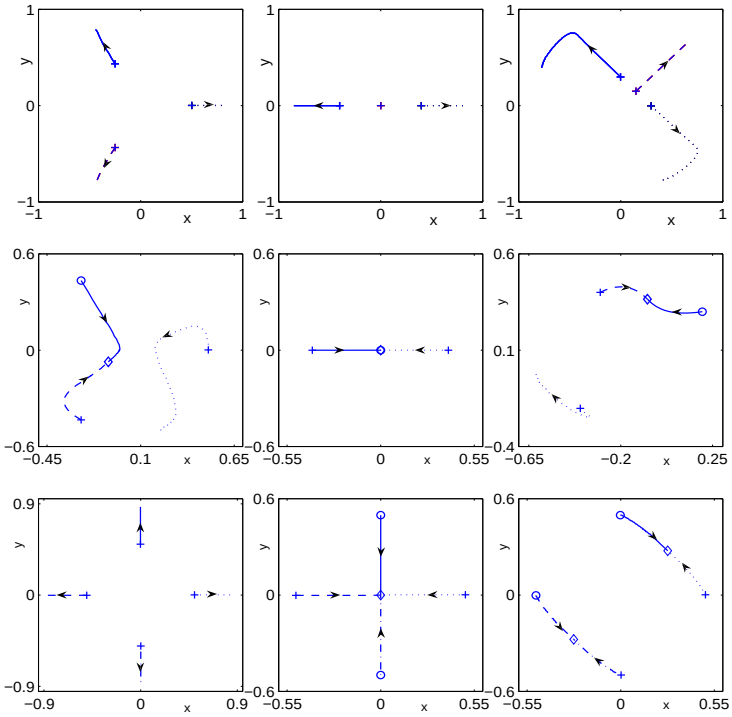

Figure 10: Trajectory of vortex centers for the interaction of different vortex lattices in GLE under Dirichlet BC with $\varepsilon=\frac{1}{32}$ and $h(\mathbf{x})=0$ for cases I-IX (from left to right and then from top to bottom) in Section 4.4.

results on a rectangular domain $\Omega=[-1.6,1.6]\times[-1,1]$ for different M and $h(\mathbf{x})$ in (4.1). In addition, Fig. 12 shows similar results with $M=8$ for different $h(\mathbf{x})$ and domain Ω.

From Figs. 11, 12 & 13 and additional numerical results not shown here for brevity, we can draw the following conclusions for the steady state patterns of vortex lattices under the GLE dynamics (1.1) with Dirichlet BC: (i). The vortex undergo repulsive interaction between each other and they move to locations near the boundary of Ω, there is no collision and a steady state pattern is formed when $t\to\infty$. In fact, the steady state is also the solution of the following minimization problem

$$\phi^{\varepsilon}=\text{argmin}_{\phi(\mathbf{x})|_{\mathbf{x}\in\partial\Omega}=\psi_0^{\varepsilon}(\mathbf{x})|_{\mathbf{x}\in\partial\Omega}}\mathcal{E}^{\varepsilon}(\phi).$$

(ii). During the dynamics, the GL functional decreases when time increases. (iii). Both the geometry of the domain and the boundary condition, i.e. $h(\mathbf{x})$, affect the final steady states significantly. The configuration of a vortex lattice at the steady state follows the symmetry of Ω and $h(\mathbf{x})$. For example, in the disk domain, when $h(\mathbf{x})=x^2-y^2+2xy$, the vortex lattice is symmetric with respect to the two lines $y=(1-\sqrt{2})x$ and $y=(1+\sqrt{2})x$ which satisfy $h(\mathbf{x})=0$ (cf. Fig. 11). (iv). At the steady state, the distance between the vortex centers and $\partial\Omega$ depends on ε and M. For fixed M, when ε decreases, the distance decreases; and respectively, for fixed ε, when M increases, the distance decreases. In

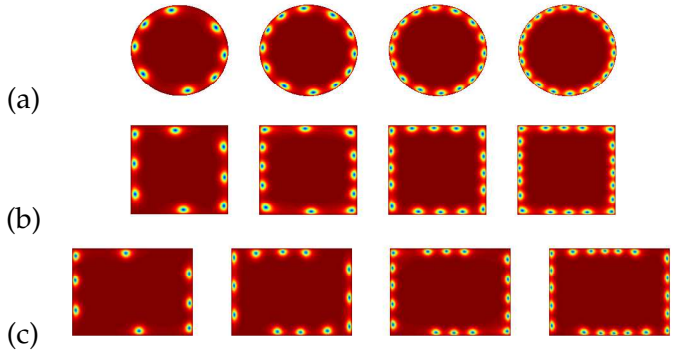

Figure 11: Contour plots of $|\phi^\varepsilon(\mathbf{x})|$ for the steady states of vortex lattice in GLE under Dirichlet BC with $\varepsilon=\frac{1}{16}$ for $M=8,12,16,20$ (from left column to right column) and different domains: (a) unit disk $\Omega=B_1(\mathbf{0})$, (b) square domain $\Omega=[-1,1]^2$, (c) rectangular domain $\Omega=[-1.6,1.6]\times[-1,1]$.

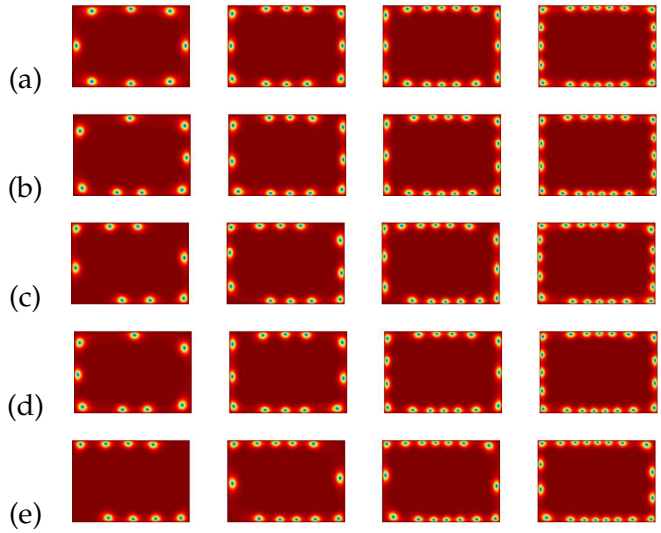

Figure 12: Contour plots of $|\phi^\varepsilon(\mathbf{x})|$ for the steady states of vortex lattice in GLE under Dirichlet BC with $\varepsilon=\frac{1}{16}$ on a rectangular domain $\Omega=[-1.6,1.6]\times[-1,1]$ for $M=8,12,16,20$ (from left column to right column) and different $h(\mathbf{x})$: (a) $h(\mathbf{x})=0$, (b) $h(\mathbf{x})=x+y$, (c) $h(\mathbf{x})=x^2-y^2$, (d) $h(\mathbf{x})=x-y$, (e) $h(\mathbf{x})=x^2-y^2-2xy$.

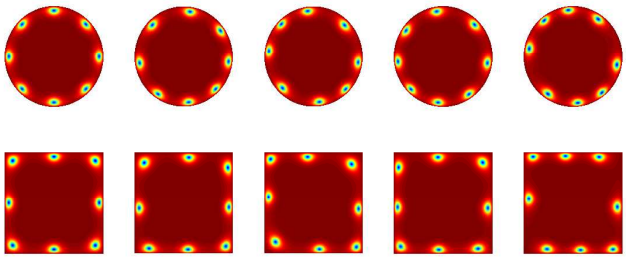

Figure 13: Contour plots of $|\phi^\varepsilon(\mathbf{x})|$ for the steady states of vortex lattice in GLE under Dirichlet BC with $\varepsilon=\frac{1}{16}$ and $M=8$ on a unit disk $\Omega=B_1(\mathbf{0})$ (top row) or a square $\Omega=[-1,1]^2$ (bottom row) under different $h(\mathbf{x})=0, x+y, x^2-y^2, x-y, x^2-y^2-2xy$ (from left column to right column).

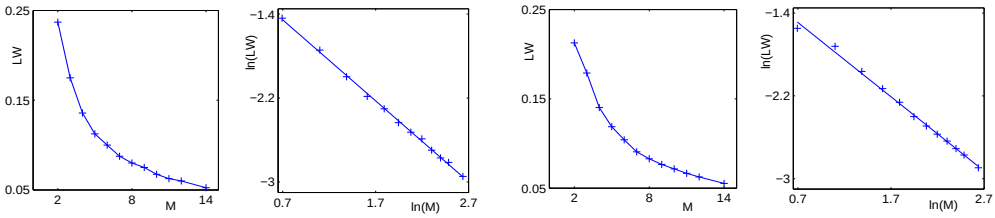

Figure 14: Width of the boundary layer LW vs M (the number of vortices) under Dirichlet BC on a square $\Omega=[-1,1]^2$ when $\varepsilon=\frac{1}{16}$ for different $h(\mathbf{x})$: $h(\mathbf{x})=0$ (left two), $h(\mathbf{x})=x+y$ (right two).

order to characterize this distance, we denote

$$LW := LW(M,\varepsilon) = \lim_{t\to\infty} \min_{1\le j\le M} \operatorname{dist}(\mathbf{x}_j^\varepsilon(t),\partial\Omega), \qquad M\ge 2.$$

For a square domain $\Omega=[-1,1]^2$, we find these distances numerically and depict $LW(M,\varepsilon)$ with $\varepsilon=\frac{1}{16}$ for different M in Fig. 14. From these results, we can fit the following relations between $LW(M,\varepsilon=1/16)$ as a function of M as

$$\mathrm{LW}\approx 0.4M^{-0.7713}, \qquad M\gg 1,$$

for $h(\mathbf{x})\equiv 0$, and respectively,

$$\mathrm{LW}\approx 0.3714M^{-0.7164}, \qquad M\gg 1,$$

for $h(\mathbf{x})=x+y$. For other cases, we can also fit out similar results, we omit here for brevity.

5 Numerical results under homogeneous Neumann BC

In this section, we report numerical results for vortex interactions of GLE (1.1) under the homogeneous Neumann BC (1.4) and compare them with those obtained from the reduced dynamical laws (2.20) with (2.3). The initial condition ψ_0^ε in (1.2) is chosen as

$$\psi_0^\varepsilon(\mathbf{x}) = \psi_0^\varepsilon(x,y) = e^{ih_n(\mathbf{x})}\prod_{j=1}^{M}\phi_{n_j}^\varepsilon(\mathbf{x}-\mathbf{x}_j^0), \qquad \mathbf{x}=(x,y)\in\bar{\Omega}; \tag{5.1}$$

which is similar as the one defined in equation (4.1) by only replacing the harmonic function $h(\mathbf{x})$ there with $h_n(\mathbf{x})$ defined as

$$\Delta h_n(\mathbf{x}) = 0, \quad \mathbf{x}\in\Omega, \qquad \int_\Omega h_n(\mathbf{x})d\mathbf{x} = 0,$$

with Neumann BC

$$\frac{\partial}{\partial\mathbf{n}}h_n(\mathbf{x}) = -\frac{\partial}{\partial\mathbf{n}}\sum_{l=1}^{M} n_l\theta(\mathbf{x}-\mathbf{x}_l), \qquad \mathbf{x}\in\partial\Omega.$$

The GLE (1.1) with (1.4), (1.2) and (5.1) is solved by the method TSCP presented in Section 3.

5.1 Single vortex

Here we present numerical results of the motion of a single quantized vortex in the GLE (1.1) dynamics and its corresponding reduced dynamics, i.e. we take $M=1$ and $n_1=1$ in (5.1). Fig. 15 depicts trajectory of the vortex center for different $\mathbf{x}_1^0$ in (5.1) when $\varepsilon=\frac{1}{32}$ in (1.1) and d_1^ε for different ε. From Fig. 15 and additional numerical results not shown here for brevity, we can see that: (i). The initial location of the vortex, i.e. value of $\mathbf{x}_0$ affects the motion of the vortex a lot and this shows the effect on the vortex from the Neumann BC. (ii). If $\mathbf{x}_1^0=(x_0,y_0)\neq(0,0)$ satisfied $x_0=0$ or $y_0=0$ or $x_0=\pm y_0$, the trajectory is a straight line. (iii). If $\mathbf{x}_1^0=(0,0)$, the vortex will not move all the time, otherwise, the vortex will move and finally exit the domain and never come back. This is quite different from the situations in bounded domain with Dirichlet BC where a single vortex can never move outside the domain or in the whole space where a single vortex doesn't move at all under the initial condition (5.1) when $\Omega=\mathbb{R}^2$. (iv). As $\varepsilon\to 0$, the dynamics of the vortex center under the GLE dynamics converges uniformly in time to that of the reduced dynamical laws well before it exits the domain, which verifies numerically the validation of the reduced dynamical laws in this case. Certainly, when the vortex center is being exited the domain or after it moves out of the domain, the reduced dynamics laws are no longer valid. However, the dynamics of GLE is still physically interesting. In fact, based on our extensive numerical experiments, the motion of the vortex center from the reduced dynamical laws agree with that from the GLE dynamics qualitatively when $0<\varepsilon<1$ and quantitatively when $0<\varepsilon\ll 1$ well before it moves out of the domain.

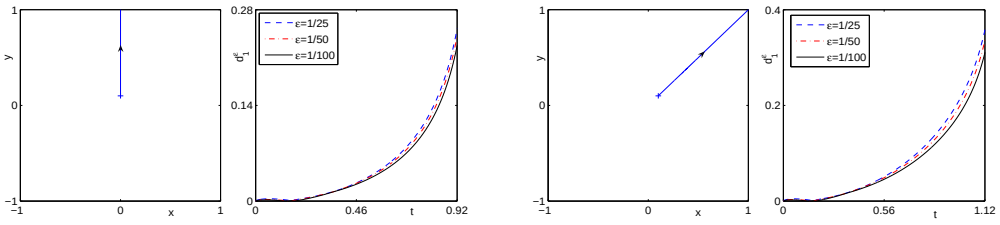

Figure 15: Trajectory of the vortex center when $\varepsilon=\frac{1}{32}$ (1st and 3rd figures) and d_1^ε for different ε (2nd and 4th figures) for the motion of a single vortex in GLE under homogeneous Neumann BC with different $\mathbf{x}_1^0$ in (5.1): $\mathbf{x}_1^0=(0,0.1)$ (left two), $\mathbf{x}_1^0=(0.1,0.1)$ (right two).

5.2 Vortex pair

Here we present numerical results of the interaction of vortex pair under the GLE (1.1) dynamics and its corresponding reduced dynamical laws, i.e. we take $M=2$, $n_1=n_2=1$, $\mathbf{x}_1^0=(-0.5,0)$ and $\mathbf{x}_2^0=(0.5,0)$ in (5.1). Fig. 16 depicts time evolution of the amplitude $|\psi^\varepsilon|$, time evolution of the GL functionals, $\mathbf{x}_1^r(t)$, $\mathbf{x}_1^\varepsilon(t)$ and $d_1^\varepsilon(t)$, and trajectory of the vortex centers for GLE under homogeneous Neumann BC.

From Fig. 16 and additional numerical results not shown here for brevity, we can draw

the following conclusions for the interaction of vortex pair under the GLE dynamics (1.1) with homogeneous Neumann BC: (i). The two vortices undergo a repulsive interaction, their centers move outwards along the line connected them initially with symmetric trajectories, i.e. $\mathbf{x}_1^\varepsilon(t) = -\mathbf{x}_2^\varepsilon(t)$ (cf. Fig. 16 (a) & (b)). Moreover, if the two vortices are not located symmetrically initially, the one closer to the boundary will first move outside the domain and the other one will exit the domain later. All the vortices will exit the domain Ω at finite time T_ε which increases when ε decreases. (ii). When $\varepsilon \to 0$, the dynamics of the two vortex centers under the GLE dynamics converge uniformly in time to that of the reduced dynamical laws before any one of them exit the domain (cf. Fig. 16(c)), which verifies numerically the validation of the reduced dynamical laws in this case. In fact, based on our extensive numerical experiments, the motion of the two vortex centers from the reduced dynamical laws agree with those from the GLE dynamics qualitatively when $0 < \varepsilon < 1$ and quantitatively when $0 < \varepsilon \ll 1$. (iii). During the dynamics of GLE, the GL functional and its kinetic parts decrease when time increases, its interaction part doesn't change much when t is small and changes dramatically when any one of the two vortices move outside the domain Ω. When $t \to \infty$, all the three quantities converge to 0 (cf. Fig. 16(c)), which imply that a constant steady state will be reached in the form of $\phi^\varepsilon(\mathbf{x}) = e^{ic_0}$ for $\mathbf{x} \in \Omega$ with c_0 a constant.

5.3 Vortex dipole

Here we present numerical results of the interaction of vortex dipole under the GLE (1.1) dynamics and its corresponding reduced dynamical laws, i.e. we take $M = 2$, $n_1 = -1$, $n_2 = 1$, $\mathbf{x}_1^0 = (-d_0, 0)$ and $\mathbf{x}_2^0 = (d_0, 0)$ with d_0 a constant.

Fig. 17 depicts contour plots of the amplitude $|\psi^\varepsilon|$, while Fig. 18 shows time evolution of GL functionals and trajectory of the vortex centers when $\varepsilon = \frac{1}{32}$ in (1.1) for different d_0 in (5.1). Fig. 19 shows time evolution of $\mathbf{x}_1^r(t)$, $\mathbf{x}_1^\varepsilon(t)$ and $d_1^\varepsilon(t)$ for different ε and d_0.

From Figs. 17, 18 & 19 and additional numerical results not shown here for brevity, we can draw the following conclusions for the interaction of vortex dipole under the GLE dynamics (1.1) with homogeneous Neumann BC: (i). The initial location of the vortices, i.e. d_0, affects the motion of vortices significantly. In fact, there exists a critical value $d_c^r = d_c^\varepsilon$ for $0 < \varepsilon < 1$, which is found numerically as $d_c^r = 0.5$, such that when the distance between the two vortex centers initially $d_0 = \frac{1}{2}|\mathbf{x}_1^0 - \mathbf{x}_2^0| < d_c^r$, then the two vortices will move towards each other along the line connecting their initial locations and finally merge at the origin at finite time T_ε which increases when ε decreases, and respectively, when $d_0 > d_c^r$, the two vortices will move outwards along the line connecting their initial locations and finally move out of the domain at finite time T_ε which increases when ε decreases (cf. Figs. 17 & 18). Moreover, the trajectories of the two vortices are symmetric i.e. $\mathbf{x}_1(t) = -\mathbf{x}_2(t)$, and finally the GLE dynamics will lead to a constant steady state with amplitude 1, i.e. $\phi^\varepsilon(\mathbf{x}) = e^{ic_0}$ for $\mathbf{x} \in \Omega$ with c_0 a real constant. (ii). When $\varepsilon \to 0$, the dynamics of the two vortex centers under the GLE dynamics converges uniformly in time to that of the reduced dynamical laws before they collide or move out of the domain (cf. Fig. 19)

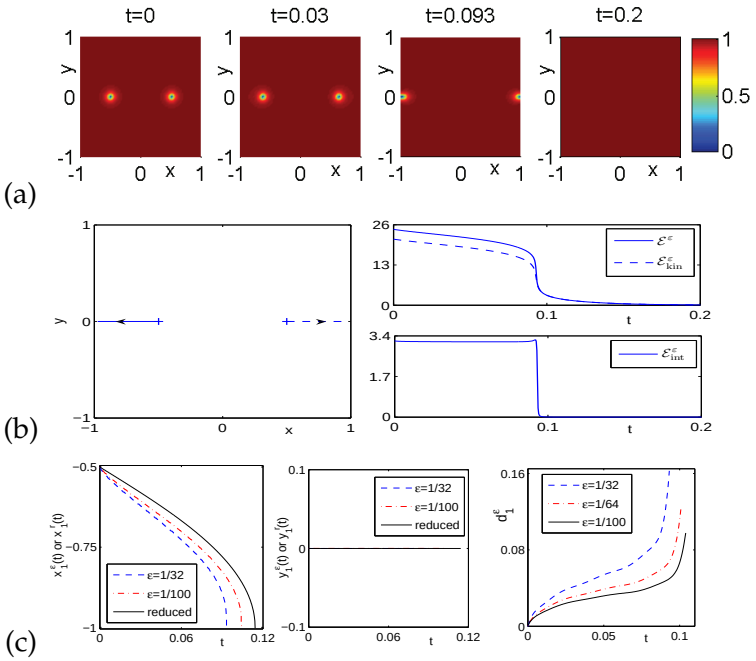

Figure 16: Dynamics and interaction of a vortex pair in GLE under Neumann BC: (a) contour plots of $|\psi^\varepsilon|$ with $\varepsilon=\frac{1}{32}$ at different times, (b) trajectory of the vortex centers (left) and time evolution of the GL functionals (right) for $\varepsilon=\frac{1}{32}$, (c) time evolution of $\mathbf{x}_1^\varepsilon(t)$ and $\mathbf{x}_1^r(t)$ (left and middle) and their difference $d_1^\varepsilon(t)$ (right) for different ε.

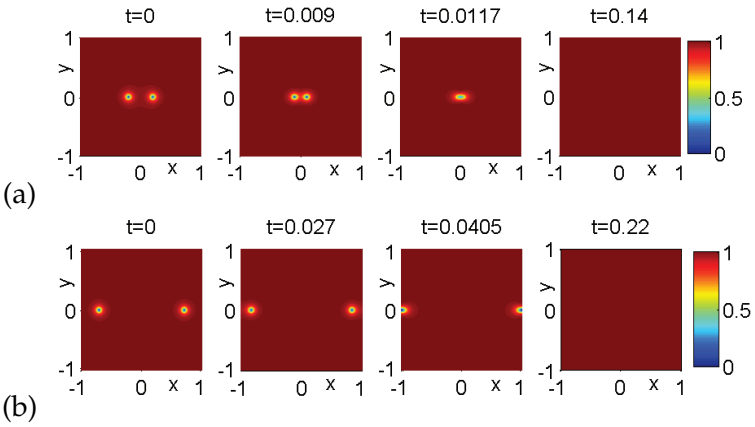

Figure 17: Contour plots of $|\psi^\varepsilon(\mathbf{x},t)|$ at different times for the interaction of vortex dipole in GLE under Neumann BC with $\varepsilon=\frac{1}{32}$ for different d_0: (a) $d_0=0.2$, (b) $d_0=0.7$.

which verifies numerically the validation of the reduced dynamical laws in this case. In fact, based on our extensive numerical experiments, the motion of the two vortex centers from the reduced dynamical laws agree with those from the GLE dynamics qualitatively when $0<\varepsilon<1$ and quantitatively when $0<\varepsilon\ll 1$. (iii) During the dynamics of GLE, the GL

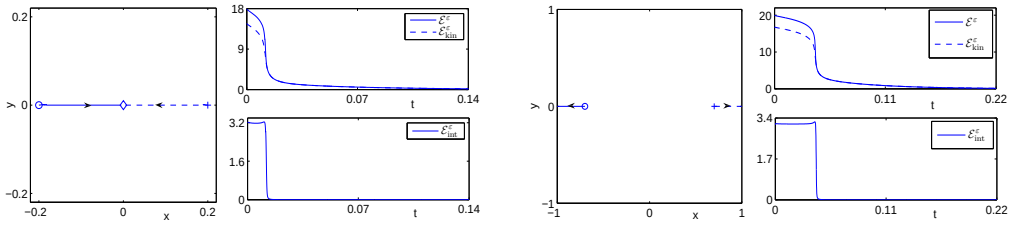

Figure 18: Trajectory of vortex centers (1rst and 3rd figures) and time evolution of the GL functionals (2nd and 4th figures) for the interaction of vortex dipole in GLE under Neumann BC with $\varepsilon=\frac{1}{32}$ for different d_0: $d_0=0.2$ (left two), $d_0=0.7$ (right two).

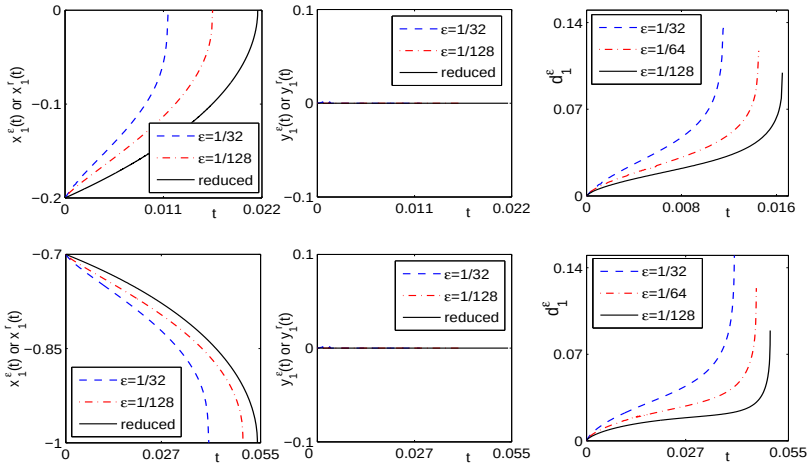

Figure 19: Time evolution of $\mathbf{x}_1^\varepsilon(t)$ and $\mathbf{x}_1^r(t)$ (left and middle) and their difference $d_1^\varepsilon(t)$ (right) for different ε and d_0: (a) $d_0=0.2$, (b) $d_0=0.7$.

functional and its kinetic part decrease when time increases, its interaction part doesn't change much when t is small. All the three quantities changes dramatically when the two vortices collide or move across $\partial\Omega$ and eventually converge to 0 when $t\to\infty$ (cf. Fig. 18).

5.4 Vortex lattices

Here we present numerical results of the interaction of vortex lattices under the GLE (1.1) dynamics. We will consider the following cases:

case I. $M=3$, $n_1=n_2=n_3=1$, $\mathbf{x}_1^0=(-0.2,\frac{\sqrt{3}}{5})$, $\mathbf{x}_2^0=(-0.2,-\frac{\sqrt{3}}{5})$, $\mathbf{x}_3^0=(0.4,0)$;

case II. $M=3$, $n_1=n_2=n_3=1$, $\mathbf{x}_1^0=(-0.4,0)$, $\mathbf{x}_2^0=(0,0)$, $\mathbf{x}_3^0=(0.4,0)$;

case III. $M=3$, $n_1=n_2=n_3=1$, $\mathbf{x}_1^0=(-0.4,0.2)$, $\mathbf{x}_2^0=(0,0.2)$, $\mathbf{x}_3^0=(0.4,0.2)$;

case IV. $M=3$, $n_2=-1$, $n_1=n_3=1$, $\mathbf{x}_1^0=(-0.4,0)$, $\mathbf{x}_2^0=(0,0)$, $\mathbf{x}_3^0=(0.4,0)$;

case V. $M=3$, $n_3=-1$, $n_1=n_2=1$, $\mathbf{x}_1^0=(-0.2,\frac{\sqrt{3}}{5})$, $\mathbf{x}_2^0=(-0.2,-\frac{\sqrt{3}}{5})$, $\mathbf{x}_3^0=(0.4,0)$;

case VI. $M=4$, $n_1=n_2=n_3=n_4=1$, $\mathbf{x}_1^0=(0.4,-0.4\sin(1))$, $\mathbf{x}_2^0=(-0.2,0.4\cos(1))$, $\mathbf{x}_3^0=(-0.2,0.4\sin(1))$, $\mathbf{x}_4^0=(0,0)$;

case VII. $M=4$, $n_1=n_3=-1$, $n_2=n_4=1$, $\mathbf{x}_1^0=(-0.4,0)$, $\mathbf{x}_2^0=(-\frac{2}{15},0)$, $\mathbf{x}_3^0=(\frac{2}{15},0)$, $\mathbf{x}_4^0=(0.4,0)$;

case VIII. $M=4$, $n_1=n_2=-1$, $n_3=n_4=1$, $\mathbf{x}_1^0=(0.4,0)$, $\mathbf{x}_2^0=(-0.2,\frac{\sqrt{3}}{5})$, $\mathbf{x}_3^0=(-0.2,-\frac{\sqrt{3}}{5})$, $\mathbf{x}_4^0=(0,0)$;

case IX. $M=4$, $n_2=n_3=1$, $n_1=n_4=-1$, $\mathbf{x}_1^0=(0.4,0)$, $\mathbf{x}_2^0=(-0.2,\frac{\sqrt{3}}{5})$, $\mathbf{x}_3^0=(-0.2,-\frac{\sqrt{3}}{5})$, $\mathbf{x}_4^0=(0,0)$.

Fig. 20 shows trajectory of the vortex centers when $\varepsilon=\frac{1}{32}$ in (1.1) for the above 9 cases. From Fig. 20 and additional numerical results not shown here for brevity, we can draw the following conclusions: (i). The interaction of vortex lattices under the GLE dynamics with homogeneous Neumann BC is very interesting and complicated. The detailed dynamics and interaction pattern of a lattice depends on its initial alignment of the lattice and geometry of the domain Ω. (ii). For a lattice of M vortices, if they have the same index, then at least $M-1$ vortices will move out of the domain at finite time and no collision will happen for any time $t\geq 0$. On the other hand, if they have opposite index, collision will happen at finite time. After collisions, the leftover vortices will then move

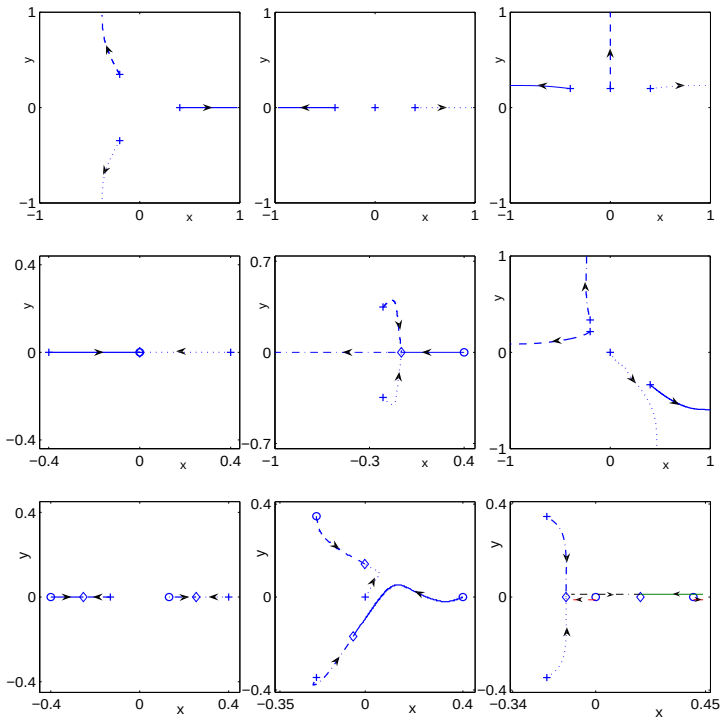

Figure 20: Trajectory of vortex centers for the interaction of different vortex lattices in GLE under homogeneous Neumann BC with $\varepsilon=\frac{1}{32}$ for cases I-IX (from left to right and then from top to bottom) in Section 5.4.

out of the domain at finite time and at most one vortex may left in the domain. When t is sufficiently large, in most cases, no vortex is left in the domain; of course, when the geometry and initial setup are properly symmetric and M is odd, there maybe one vortex left in the domain.

5.5 Steady state patterns of vortex lattices

Here we present the steady state patterns of vortex lattices under the GLE dynamics (1.1) with homogeneous Neumann BC. To this end, we take $\varepsilon=\frac{1}{16}$ in (1.1) and assume the M vortices are initially located uniformly on a line, i.e.

$$\mathbf{x}_j^0=\left(-0.5+\frac{j-1}{M-1},0\right),\qquad j=1,2,\cdots,M,$$

or on a circle with radius $R_1=0.5$, i.e.

$$\mathbf{x}_j^0=0.5\left(\cos\left(\frac{2j\pi}{M}\right),\sin\left(\frac{2j\pi}{M}\right)\right),\qquad j=1,2,\cdots,M.$$

Fig. 21 depicts the amplitude $|\psi^\varepsilon|$ of the initial data and final steady states under the GLE dynamics with different initial setups.

From Fig. 21 and additional numerical results not shown here for brevity, we can draw the following conclusions for the interaction of vortex lattices under the GLE dynamics (1.1) with homogeneous Neumann BC: (i). If the three like vortices initially located uniformly on a circle, they will repel each other and finally exit outside the domain and never come back. (ii). If the three like vortices initially located uniformly on a line, the left and right vortices will finally exit outside the domain and never come back, while

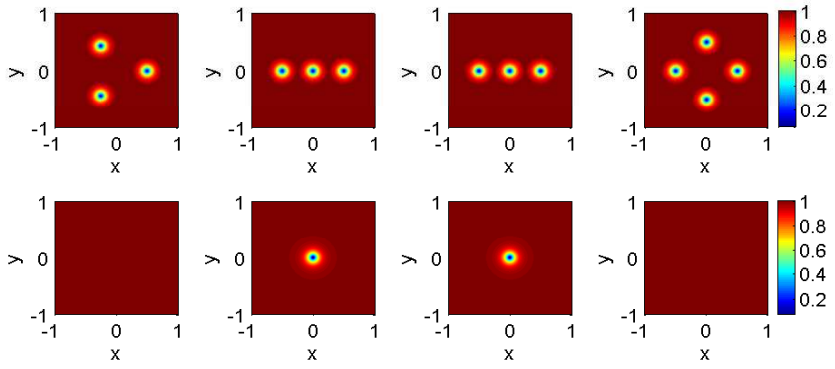

Figure 21: Contour plots of the amplitude $|\psi^\varepsilon|$ for the initial data (top) and corresponding steady states (bottom) of vortex lattice in the GLE (1.1) under homogeneous Neumann BC with $\varepsilon=\frac{1}{16}$ for different number of vortices M and winding number n_j: $M=3,n_1=n_2=n_3=1$ (first and second columns); $M=3,n_1=-n_2=n_3=1$ (third column); and $M=4,n_1=-n_2=n_3=-n_4=1$ (fourth column).

the middle one does not move all the time. (iii). If the three vortices initially located uniformly on a line with the middle vortex whose winding number is opposite to the other two, the middle one will not move all the time, while the left and right vortices will move toward the origin and one of them will merge with the middle vortex, finally only one vortex will stay at the origin forever. (iv). If the four vortices initially located uniformly on a circle with the sign of winding number alternatively changed, the four vortices will move toward the original point and merge with each other, and finally there will be no vortex in the domain. (v). Actually, from our extensive numerical experiments, we can conclude that for any initial setup, if the number of vortices M is even, the vortices will either merge or move outside the domain, and finally there will be no vortex leftover in the domain; while if M is odd, there will be at most one vortex leftover in the domain when $t \to \infty$.

6 Conclusion

By presenting efficient and accurate numerical methods for discretizing the Ginzburg-Landau equation (GLE) with a dimensionless parameter $0 < \varepsilon < 1$ on boundary domains with either Dirichlet or homogenous Neumann BC and its corresponding reduced dynamical laws, we studied numerically quantized vortex interaction in GLE for superconductivity and compared numerically vortex interaction patterns between the GLE dynamics and its corresponding reduced dynamical laws under different initial setups. Based on extensive numerical results, we verified that the dynamics of vortex centers under the GLE dynamics converges to that of the reduced dynamical laws when $\varepsilon \to 0$ before they collide and/or move out of the domain. Certainly, after either vortices collide with each other or move out of the domain, the reduced dynamical laws are no longer valid; however, the dynamics and interaction of quantized vortices are still physically interesting and they can be obtained from the direct numerical simulations for the GLE with fixed $\varepsilon > 0$ even after they collide and/or move out of the domain. We also identified the parameter regimes where the reduced dynamical laws agree with qualitatively and/or qualitatively as well as fail to agree with those from the GLE dynamics. Some very interesting nonlinear phenomena related to the quantized vortex interactions in the GLE for superconductivity were also observed from our direct numerical simulation results of GLE. Different steady state patterns of vortex lattices under the GLE dynamics were obtained numerically. From our numerical results, we observed that boundary conditions and domain geometry affect significantly on vortex dynamics and interaction, which showed different interaction patterns compared to those in the whole space case [37, 38].

Acknowledgments

This work was supported by the Singapore A*STAR SERC "Complex Systems" Research Programme grant 1224504056 and the Academic Research Fund of Ministry of Educa-

tion of Singapore grant R-146-000-120-112. Part of this work was done when the first author was visiting Beijing Computational Science Research Center in 2011 and he also acknowledges Professor Fang-Hua Lin for stimulating discussion.

References

[1] B. P. Anderson, Resource artical: Experiment with vortices in superfluid atomic gases, J. Low Temp. Phys., 161 (2010), 574-602.
[2] N. André and I. Shafrir, Asymptotic behavior for the Ginzburg-Landau functional with weight (I), Arch. Rat. Mech. Anal., 142 (1998), 45-73.
[3] N. André and I. Shafrir, Asymptotic behavior for the Ginzburg-Landau functional with weight (II), Arch. Rat. Mech. Anal., 142 (1998), 75-98.
[4] W. Bao, Numerical methods for the nonlinear Schrödinger equation with nonzero far-field conditions, Methods Appl. Anal., 11 (2004), 367-388.
[5] W. Bao, Q. Du and Y. Zhang, Dynamics of rotating Bose-Einstein condensates and their efficient and accurate numerical computation, SIAM J. Appl. Math., 66 (2006), 758-786.
[6] P. Bauman, C. N. Chen, D. Phillips and P. Sternberg, Vortex annihilation in nonlinear heat flow for Ginzburg-Landau systems, European J. Appl. Math., 6 (1995), 115-126.
[7] F. Bethuel, H. Brezis and F. Hélein, Ginzburg-Landau Vortices, Brikhäuser, Boston, 1994.
[8] S. Chapman, Q. Du and D. Gunzburger, A model for varia ble thickness superconducting thin film, Z. Angew. Math. Phys., 47 (1996), 410-431.
[9] M. del Pino, M. Kowalczyk and M. Musso, Variational reduction for Ginzburg-Landau vortices, J. Funct. Anal., 239 (2006), 497-541.
[10] R. J. Donnelly, Quantized Vortices in Helium II, Cambridge Univ., Cambridge, 1991.
[11] Q. Du and D. Gunzburger, A model for superconduction thin films having variable thickness, Phys. D., 69 (1993), 215-231.
[12] W. E, Dynamics of vortices in Ginzburg-Landau theroties with applications to superconductivity, Phys. D, 77 (1994), 38-404.
[13] R. Glowinski and P. Tallec, Augmented Lagrangian and Operator Splitting Method in Nonlinear Mechanics, SIAM, Philadelphia, PA, 1989.
[14] S. Gustafson and I. M. Sigal, Effective dynamics of magnetic vortices, Adv. Math., 199 (2006), 448-498.
[15] R. Jerrard and H. Soner, Dynamics of Ginzburg-Landau vortices, Arch. Rat. Mech. Anal., 142 (1998), 99-125.
[16] H. Jian, The dynamical law of Ginzburg-Landau vortices with a pining effect, Appl. Math. Lett., 13 (2000), 91-94.
[17] H. Jian and B. Song, Vortex dynamics of Ginzburg-Landau equations in inhomogeneous superconductors, J. Diff. Eq., 170 (2001), 123-141.
[18] H. Jian and Y. Wang, Ginzburg-Landau vortices in inhomogeneous superconductors, J. Part. Diff. Eq., 15 (2002), 45-60.
[19] S. Jimbo and Y. Morita, Stability of nonconstant steady-state solutions to a Ginzburg-Landau equation in higer space dimension, Nonlinear Anal.: T.M.A., 22 (1994), 753-770.
[20] S. Jimbo and Y. Morita, Vortex dynamics for the Ginzburg-Landau equation with Neumann condition, Methods App. Anal., 8 (2001), 451-477.
[21] S. Jimbo and Y. Morita, Notes on the limit equation of vortex equation of vortex motion for the Ginzburg-Landau equation with Neumann condition, Japan J. Indust. Appl. Math., 18 (1972), 151-200.

[22] D. Kincaid and W. Cheney, Numerical Analysis, Mathematics of Scientific Computing, Brooks-Cole, 3rd edition, 1999.
[23] F. Lin, Some dynamical properties of Ginzburg-Landau vortices, Comm. Pure Appl. Math., 49 (1996), 323-359.
[24] F. Lin, A remark on the previous paper "Some dynamical properties of Ginzburg-Landau vortices", Comm. Pure Appl. Math., 49 (1996), 361-364.
[25] F. Lin, Complex Ginzburg-Landau Equations and Dynamics of Vortices, Filaments, and Codimension-2 Submanifolds, Comm. Pure Appl. Math., 51 (1998), 385-441.
[26] F. Lin, Mixed vortex-antivortex solutions of Ginzburg-Landu equations, Arch. Rat. Mech. Anal., 133 (1995), 103-127.
[27] F. Lin and Q. Du, Ginzburg-Landau vortices: Dynamics, pining and hysteresis, SIAM J. Math. Anal., 28 (1997), 1265-1293.
[28] J. Neu, Vortices in complex scalar fields, Phys. D, 43 (1990), 385-406.
[29] L. Peres and J. Rubinstein, Vortex dynamics for U(1)-Ginzburg-Landau models, Phys. D, 64 (1993), 299-309.
[30] J. Rubinstein and P. Sternberg, On the slow motion of vortices in the Ginaburg-Landau heat flow, SIAM J. Appl. Math., 26 (1995), 1452-1466.
[31] E. Sandier and S. Serfaty, Gamma-convergence of gradient flows with applications to Ginzburg-Landau, Comm. Pure Appl. Math., 57 (2004), 1627-1672.
[32] S. Serfaty, Stability in 2D Ginzburg-Landau pass to the limit, Indiana U. Math. J., 54 (2005), 199-221.
[33] S. Serfaty, Vortex collisions and energy-dissipation rates in the Ginzburg-Landau heat flow. Part II: the dynamics, J. Euro. Math. Soc., 9 (2007), 383-426.
[34] J. Shen and T. Tang, Spectral and High-Order Method with Applications, Science Press, 2006.
[35] G. Strang, On the construction and comparision of difference schemes, SIAM J. Numer. Anal., 5 (1968), 505-517.
[36] M. I. Weinstein and J. Xin, Dynamic stability of vortex solutions of Ginzburg-Landau and nonlinear Schrödinger equations, Comm. Math. Phys., 180 (1996), 389-428.
[37] Y. Zhang, W. Bao and Q. Du, Numerical simulation of vortex dynamics in Ginzburg-Landau-Schrödinger equation, Euro. J. Appl. Math., 18 (2007), 607-630.
[38] Y. Zhang, W. Bao and Q. Du, The dynamics and interactions of quantized vortices in Ginzburg-Landau-Schrödinger equation, SIAM I. Appl. Math., 67 (2007), 1740-1775.